© 2023. Published by The Company of Biologists Ltd | Development (2023) 150, dev201335. doi:10.1242/dev.201335

RESEARCH ARTICLE

Molecular mechanism of synovial joint site specification and induction in developing vertebrate limbs

Upendra S. Yadav[1,2,§,¶], Tathagata Biswas[1,2,‡,§], Pratik N. Singh[1,2,*], Pankaj Gupta[1,2], Soura Chakraborty[1], Irene Delgado[3,4], Hamim Zafar[1,2,5], Terence D. Capellini[6,7], Miguel Torres[3,4] and Amitabha Bandyopadhyay[1,2,¶]

ABSTRACT

The vertebrate appendage comprises three primary segments, the stylopod, zeugopod and autopod, each separated by joints. The molecular mechanisms governing the specification of joint sites, which define segment lengths and thereby limb architecture, remain largely unknown. Existing literature suggests that reciprocal gradients of retinoic acid (RA) and fibroblast growth factor (FGF) signaling define the expression domains of the putative segment markers *Meis1*, *Hoxa11* and *Hoxa13*. *Barx1* is expressed in the presumptive joint sites. Our data demonstrate that RA-FGF signaling gradients define the expression domain of *Barx1* in the first presumptive joint site. When misexpressed, Barx1 induces ectopic interzone-like structures, and its loss of function partially blocks interzone development. Simultaneous perturbations of RA-FGF signaling gradients result in predictable shifts of *Barx1* expression domains along the proximo-distal axis and, consequently, in the formation of repositioned joints. Our data suggest that during early limb bud development in chick, *Meis1* and *Hoxa11* expression domains are overlapping, whereas the *Barx1* expression domain resides within the *Hoxa11* expression domain. However, once the interzone is formed, the expression domains are refined and the *Barx1* expression domain becomes congruent with the border of these two putative segment markers.

KEY WORDS: RA/FGF signaling, Barx1, Cartilage segmentation, Limb patterning, Synovial joints

INTRODUCTION

During vertebrate embryogenesis, the limb is initially perceptible as a small bud containing a single cartilaginous anlage that grows in length and undergoes repeated branching and segmentation, to eventually give rise to almost all of the mature skeletal elements. Segmentation of the limb skeletal anlage gives rise to three distinct segments: the upper limb (stylopod), the lower limb (zeugopod) and the hand/foot (autopod) (Oster et al., 1988). Across vertebrates, the length ratios of these segments considerably vary to accommodate functional locomotor and positional behavioral differences between species (e.g. human versus bat). The length ratios of each of these three distinct segments depend on the correct specification of a segmentation site or future joint within the cartilaginous skeletal template. It is well known that the proximal joint (i.e. elbow or knee) is determined first with more distal joints (i.e. wrist or ankle) forming later. This progressive specification is linked to the proximo-distal (P-D) patterning of skeletal elements, as proposed by the two-signal model (Tabin and Wolpert, 2007), albeit the precise mechanism is unclear.

According to the two-signal model, limb P-D patterning is determined by reciprocal antagonism between two diffusible signals: retinoic acid (RA), which is secreted from the limb flank, and fibroblast growth factors (FGFs), which are secreted from the distal epithelial structure called the apical ectoderm ridge (AER). Mutual antagonism, coupled with growth-induced separation of these two signaling centers, leads to dynamic changes in gene expression profile, eventually resulting in nested expression of a set of transcription factors along the proximo-distal axis of the limb – Meis1/2 (proximal), Hoxa11 (intermediate) and Hoxa13 (distal) (Mercader et al., 1999; Nelson et al., 1996). It was speculated that a joint is induced at the border of the expression domain of two adjacent segment markers (Galloway et al., 2009). Lineage tracing experiments in chick and mouse have failed to demonstrate a strict correlation between the expression of a proposed segment marker and the founder cell population for the segments (Delgado et al., 2020; Sato et al., 2007; Scotti et al., 2015). Such non-congruity has also been reported in invertebrate limb development (Milán and Cohen, 2000). Furthermore, Meis1/2 compound loss of function abolishes condensation of the stylopod, whereas zeugopod development is largely impaired (Delgado et al., 2020). On the other hand, the loss of Hox11 activity leads to the formation of dramatically short zeugopodial elements, due to a failure in the formation of the normal growth plate at the two ends of zeugopod bones. However, the zeugopod primordia are specified normally (Boulet and Capecchi, 2004; Fromental-Ramain et al., 1996). Taken together, it appears that none of these genes is individually important for specifying segment identities. Furthermore, the recent data from our group and earlier studies show that the expression of *Meis1/2* precedes the expression of *Hoxa11* and *Hoxa13* in the developing limb bud, and double conditional knockout of Meis1/2 alters the expression domains of *Hoxa11* and *Hoxa13*, suggesting that Meis1/2 dictates the establishment of the proximo-distal pattern of the limb bud (Delgado et al., 2020; Mercader et al., 1999; Nelson et al., 1996).

Expression of several known joint markers, such as *Gdf5*, *Atx* and *Jun*, has been reported at the segmentation sites, but how the

[1]Department of Biological Sciences and Bioengineering, Indian Institute of Technology Kanpur, Kanpur, Uttar Pradesh 208016, India. [2]The Mehta Family Centre for Engineering in Medicine, Indian Institute of Technology Kanpur, Kanpur, Uttar Pradesh 208016, India. [3]Cardiovascular Regeneration Program, Centro Nacional de Investigaciones Cardiovasculares, CNIC, 28029 Madrid, Spain. [4]CIBER of Cardiovascular Diseases (CIBERCV), ISCIII, 28029 Madrid, Spain. [5]Department of Computer Science and Engineering, Indian Institute of Technology Kanpur, Kanpur, Uttar Pradesh 208016, India. [6]Department of Human Evolutionary Biology, Harvard University, 11 Divinity Avenue, Cambridge, MA 02138, USA. [7]Broad Institute of MIT and Harvard, Cambridge, MA 02138, USA.
*Present address: Department of Medical Oncology and Center for Functional Cancer Epigenetics, Dana-Farber Cancer Institute, Harvard Medical School, Boston, MA 02215, USA. ‡Present address: Stowers Institute for Medical Research, Kansas City, MO 64110, USA.
§These authors contributed equally to this work

¶Authors for correspondence (upendray@iitk.ac.in; abandopa@iitk.ac.in)

T.B., 0000-0002-4067-3643; S.C., 0000-0002-3653-9652; H.Z., 0000-0002-1617-2806; A.B., 0000-0002-0429-438X

Handling Editor: Patrick Tam
Received 30 September 2022; Accepted 25 May 2023

Development (2023) 150, dev201335. doi:10.1242/dev.201335

segment-specific homeobox genes induce joint structures at their boundaries, if at all, remains unknown (Kan and Tabin, 2013; Storm and Kingsley, 1999). Finally, to date, no gene has been identified to induce the characteristic features of a joint, including the flattening of cartilage cells and eventual segmentation.

To investigate how segmentation sites (future joints) in the limbs are specified, we modelled our work on findings from vertebrate somitogenesis (Dubrulle and Pourquié, 2004) due to the remarkable similarity in segmentation and the signaling gradients across a tissue. During somitogenesis, single contiguous pre-somitic mesoderm (PSM) undergoes repetitive segmentation events to form discrete somites along the anterior-posterior (A-P) axis. This process is controlled by reciprocal gradients of RA and FGF signaling, which dictate the sites of PSM segmentation in the AP axis wherein RA signaling induces differentiation and FGF signaling keeps the PSM cells in a proliferative state (Dubrulle and Pourquié, 2004). Therefore, we hypothesized that, akin to the segmentation of presomitic mesoderm, the reciprocal RA and FGF signaling gradients in the developing limb bud regulate the position of the putative joint site (Fig. S1).

In this article, we identify the homeodomain-containing transcription factor *Barx1* as a molecule that is expressed in all the presumptive interzone sites in a developing limb, and its misexpression is sufficient to induce an ectopic interzone. Furthermore, we show that RA and FGF signaling gradients, together, specify the expression domain of Barx1 in the first presumptive interzone site, and thereby specify the knee joint site. We demonstrate that the *Barx1* expression domain is not induced at the border of *Meis1* and *Hoxa11* expression domains at the early stages of limb development. However, subsequent to interzone formation, the *Barx1* expression domain is coincident with the border of *Meis1* and *Hoxa11* expression domains. Our data suggest that RA-FGF signaling gradients independently control the expression domains of the putative segment markers and *Barx1*; only after interzone induction are these domains are further refined to demarcate specific segments and their borders.

RESULTS

Perturbing only RA or only the FGF signaling gradient does not alter skeletal element length ratios

We perturbed the RA-FGF signaling gradient using the classical bead implantation technique. We first implanted individual beads soaked in varying concentrations of RA or DEAB (reversible RA signaling inhibitor) in the proximal end, or FGF8 or SU5402 (FGFR1 inhibitor) in the distal end in HH20-21 chick hind limb buds (Hamburger and Hamilton, 1951; Mohammadi et al., 1997; Sachidanandan et al., 2008). We investigated the lengths of the femur (stylopod) and tibia (zeugopod), and their length ratios after HH30, i.e. once all the skeletal elements are defined. Implantation of individual beads gave normal limbs with no significant change in femur-tibia length ratios (Fig. S2A-C,A′-D′). Higher doses of SU5402 (250 µM or above) resulted in limb truncations (Fig. S2D).

Simultaneously perturbing both RA and FGF signaling alters femur-tibia length ratios

To further explore the roles of these factors, we next attempted to perturb both signaling gradients such that the activity of one signaling pathway was raised at one end while simultaneously reducing the activity of the other signaling pathway at the other end. Through the use of progressively lower concentrations of individual chemicals, we eventually optimized pairs of concentrations such that only length ratios are altered without causing perceptible skeletal abnormalities. Simultaneous implantation of a RA-soaked bead (10 µM) in the proximal end and a SU5402-soaked bead (50 µM) in the distal end resulted in the treated limbs having similar overall lengths to the contralateral control limbs. However, the treated limbs exhibited a higher femur-to-tibia length ratio compared with the contralateral control limbs (Fig. 1A,A′). The change in the femur-tibia length ratios was observed due to the increase in the length of the stylopod and simultaneous decrease in the length of the zeugopod (Table S1). In contrast, implantation of a DEAB-soaked bead (500 µM) in the proximal limb and an FGF8-soaked bead (0.1 µg/µl) in the distal limb resulted in lower femur-to-tibia length ratios compared with the untreated contralateral limb, without any gross malformation or overall size differences compared with the treated limbs (Fig. 1B,B′). This change in the femur-tibia length ratios was observed due to the decrease in the length of the stylopod and simultaneous increase in the length of the zeugopod (Table S2). Thus, manipulation of RA-FGF signaling gradients alters the relative location of the proximal-most joint site in the limb skeletal primordia.

Barx1 is expressed in presumptive interzone, interzone and articular cartilage

Changes in the ratio of the femur to tibia length may be caused by either a shift in the segmentation site of the presumptive knee joint in the early developing limb or by differential growth rates of the skeletal elements during late limb development, or a combination of both (Cooper et al., 2013). To distinguish between these possibilities, the identification of an early molecular marker of segmentation was required. The segmentation site in the cartilage anlagen is a morphologically conspicuous band of dense flat cells, referred to as the interzone. Removal of the interzone leads to the failure of segmentation and subsequent loss of joint formation (Holder, 1977). Molecularly, the interzone is characterized by the expression of genes such as *Gdf5* and *Atx* (*Enpp2*) and by the loss of *Col2a1*. However, the most frequently used markers of interzone, such as Gdf5 and Atx, are typically expressed in broader domains, which become restricted only once the interzone forms (Ray et al., 2015; Storm and Kingsley, 1999). Furthermore, none of the reported joint cartilage markers is known to induce the interzone in the developing cartilage anlage. In the context of a screen to identify genes involved in early joint development, we identified *Barx1* as an early interzone marker, the expression of which is sustained in late joints (Singh et al., 2016). This homeobox-containing gene was earlier identified to be expressed in the developing facial primordia, stomach and developing joints (Barlow et al., 1999). We found that *Barx1* expression can be detected as early as HH21-22, before segmentation occurs, in a region described as the ‘opaque patch’ or putative interzone (Fell and Canti, 1934) (Fig. 2). In corroboration, multiple Barx-binding sites were identified in an upstream enhancer region for mouse and human *Gdf5*, the mutation of which resulted in the loss of joint-specific expression of LacZ in developing joints in mouse (Chen et al., 2016). Using the chick system, we found a similar effect (Fig. S3). Because, in the developing cartilage, *Gdf5* is exclusively expressed in the interzone, our data(taken together with existing literature) suggest a potential conserved role for Barx1 in interzone induction. However, the role of Barx1 in the segmentation of limb cartilage or joint induction remains unexplored.

Barx1 is sufficient to induce ectopic interzone

To test the role of Barx1 in interzone induction, we first cloned the full-length *Barx1* gene and its constitutively active version, *Barx1*-VP16,

Development (2023) 150, dev201335. doi:10.1242/dev.201335

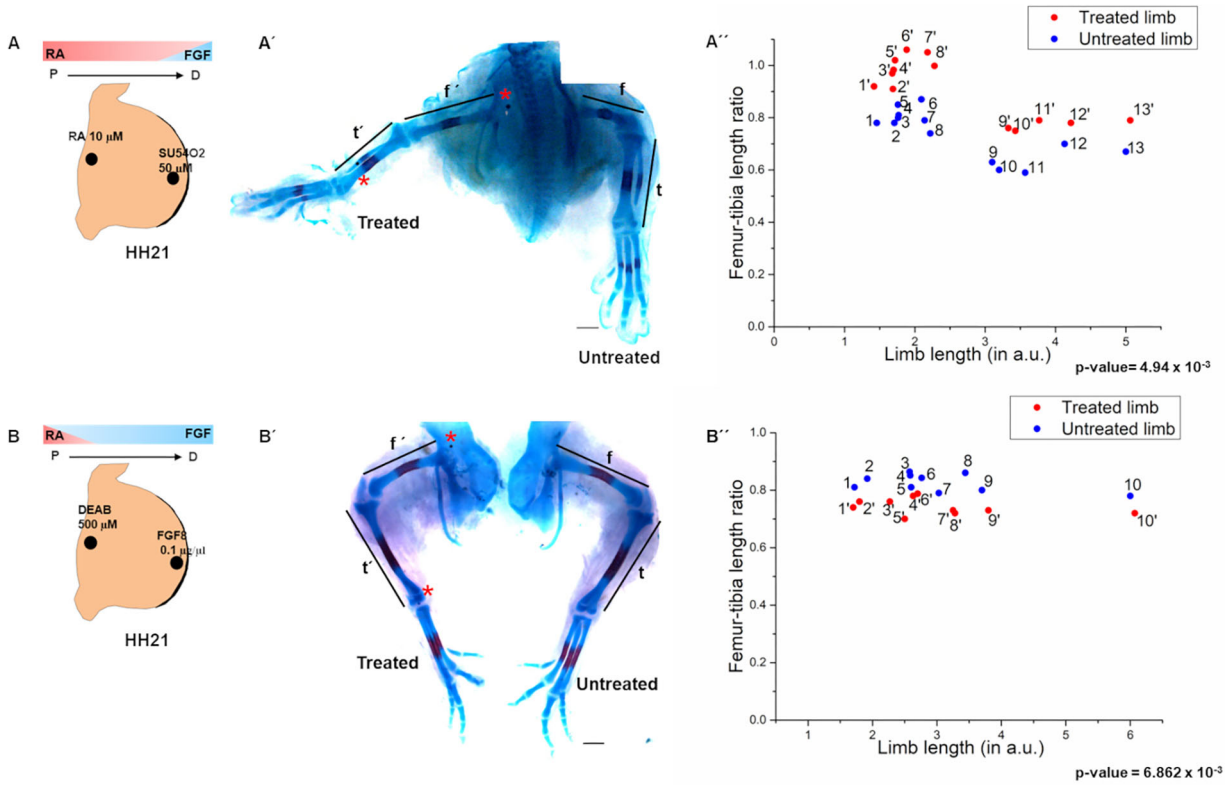

Fig. 1. Simultaneous perturbation of RA and FGF gradients alters the skeletal elements length ratio. (A,B) Bead implantation procedure. (A′,B′) Skeletal preparations from HH20-21 chick embryos, with the right hind limb-bud implanted with RA- and SU5402-soaked beads (A′), and DEAB- and FGF8 protein-soaked beads (B′), and harvested on day 8 of incubation. (A″,B″) Graphs representing femur to tibia length ratio (*y*-axis) and total limb length (*x*-axis) from treated (red, ′) and untreated (blue) limbs. Treated and untreated limbs from the same embryo are labeled with the same number. f,f′ and t,t′ represent femur and tibia lengths, respectively. Scale bars: 1 mm. One arbitrary unit (a.u.)≈5 mm. Red asterisks indicate the positions of beads.

into avian retroviral vector RCAS and then electroporated the right hind limb bud of HH14 chicken embryos with either RCAS-*Barx1* or RCAS-*Barx1*-VP16 (Logan and Tabin, 1998). Barx1 gain-of-function constructs produced grossly malformed limbs (Fig. 3A,F). Because of the severe shortening of the electroporated limbs, variations in the region and depth of infection in the developing shaft of the skeletal elements, and variations in depth of tissue under observation, it is nearly impossible to accurately identify the correct comparable regions of control limb for scrutiny. Therefore, experiments were designed to efficiently use internal controls that would eliminate contralateral and test limb mismatch problems. Internal controls have been an established method for analysis in similar studies (Hartmann and Tabin, 2001; Kumar et al., 2018). Infected cells were detected by 3C2 immunoreactivity and expression of marker genes was compared between the 3C2-positive infected cells (Fig. 3B,E,F′,I) and immediately neighboring 3C2-negative uninfected cells. Chondrocytes infected with RCAS-*Barx1* or RCAS-*Barx1*-VP16 presented with a dense, flattened interzone-like morphology

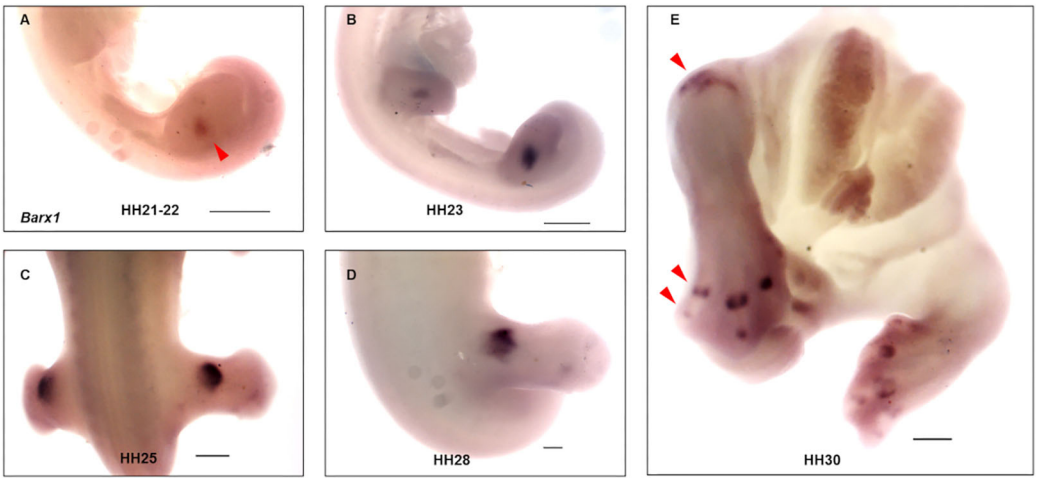

Fig. 2. Expression profile of the *Barx1* gene in developing chick limb. (A-E) The expression of *Barx1* is observed at (A) HH21-22, (B) HH23, (C) HH25, (D) HH28 and (E) HH30. The red arrowheads indicate the expression domains of *Barx1*.

Development (2023) 150, dev201335. doi:10.1242/dev.201335

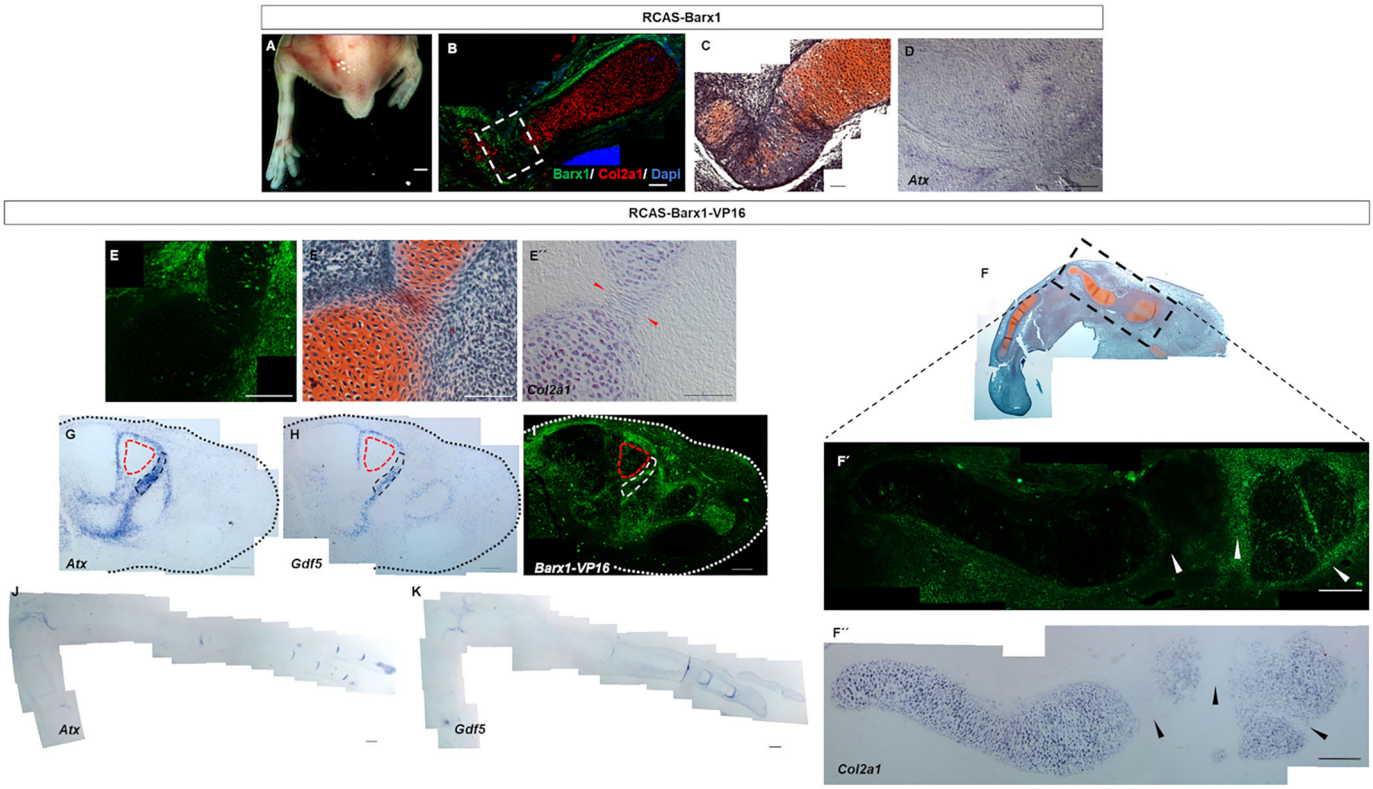

Fig. 3. Barx1 activity induces ectopic interzone-like features. (A) Chicken embryo harvested at HH34 after electroporation of the RCAS-Barx1 construct in right hind limb at HH14. The infected hind limb is short while the contralateral control limb is unaffected (*n*=8). (B) Superimposition of *in situ* hybridization for Col2a1 mRNA (red) and 3C2 immunohistochemistry (labelling RCAS-infected cells in green) on longitudinal sections of a RCAS-Barx- infected chick hind limb tibia. The area outlined indicates a region of strong RCAS infection coupled with loss of *Col2a1* mRNA expression and flattened cells. (C,D) Serial sections focusing on the infected region in B. Safranin-O staining assessing cartilage-specific proteoglycans shows loss of safranin-O stain (darker regions) along with bands of flattened cells (C). This region also shows upregulation of the interzone marker *Atx* and cell flattening (C,D). (E-E″) Cell flattening and loss of *Col2a1* in serial sections of RCAS-Barx1-VP16-infected femoral elements. (E) 3C2 staining (green) marks the cells with RCAS-Barx1-VP16 infection. (E′) A Safranin-O stained serial section exhibits cell flattening in the comparable infected region. (E″) Loss of *Col2a1* with a distinct band of flattened cells observed in another serial section in the same region as the infection area in E. (F-F″) Loss of *Col2a1* across several infected patches in the femoral element. (F) A Safranin-O stained section depicting a RCAS-Barx1-VP16 electroporated limb. (F′) 3C2 immunohistochemistry marking the infected patches in the cartilage element (white arrowheads). (F″) Loss of *Col2a1* across multiple infected patches of cartilage (black arrowheads). (G-I) Upregulation of interzone markers upon RCAS-Barx1-VP16 infection. Similar regions across serial sections are marked by dashed lines – red indicate uninfected and black indicate infection. Upregulation of both *Atx* (G) and *GDF5* (H) along the domains of RCAS-Barx1-VP16 infection marked by 3C2 immunohistochemistry (I). (J,K) *Atx* expression (J) and *Gdf5* expression (K) in the contralateral control limbs. Scale bars: 100 µm in B-I; 200 µm in J,K; 1 mm in A.

(Fig. 3C,E′); they expressed *Atx* (Fig. 3D,G) and expression of *Col2a1* was downregulated (Fig. 3B,E″,F″). Moreover, right hind limb buds co-electroporated with both RCAS-*Barx1*-VP16 and the aforementioned *Gdf5*-LacZ reporter vector, showed increased LacZ activity at these sites (Fig. S4), suggesting a role for *Barx1* in Gdf5 expression as well as in joint induction. Phenotypes observed upon RCAS-*Barx1*-VP16 electroporation (Fig. 3E-F″) were more pronounced than with RCAS-*Barx1* electroporation (Fig. 3A-D). Although RCAS-*Barx1*-VP16-infected cells (Fig. 3I) expressed *Gdf5* (Fig. 3H), we could not detect the same activity in RCAS-Barx1-infected cells. In the contralateral limbs, *Atx* and *Gdf5* expression was observed in most of the interzones (Fig. Fig. 3J,K), and the length of the contralateral limb skeleton was substantially greater than the limb skeletons electroporated with Barx1 gain-of-function constructs (compare the scale bars in Fig. 3J,K with this in Fig. 3F′,F′′). In addition, although in the contralateral limb skeleton, these markers were expressed in domains parallel to each other, in the RCAS-Barx1 infected skeletons, the expression pattern was irregular and confined to the infected domains. In order to test the necessity of Barx1 in interzone induction, we attempted to knockdown *Barx1* levels using RNA interference, following methods described by Singh et al. (2018), and using CRISPR- mediated knockout in chick (Cong et al., 2013) and mouse (Roh et al., 2018). However, none of these approaches worked. The Barx1 ORF has 69.1% GC content, with some long stretches having up to 80% GC content. For this work, we could not RT-PCR amplify the Barx1 ORF. We had to synthesize the gene chemically. It is possible that RNA interference- or CRISPR-mediated gene knockout failed due to the high GC content in the ORF (Reynolds et al., 2004; Shojaei Baghini et al., 2021). Therefore, to investigate the effect of loss of Barx1 function, we cloned a dominant-negative version of Barx1 (Barx1-ENGR, created by in-frame fusion of Barx1 with Engrailed transcriptional repressor domain) in the RCAS backbone and performed electroporation as described previously (Kamei et al., 2011). Barx1-ENGR mis-expression in the interzone region exhibits mutually exclusive domains of Barx1-ENGR expression and interzone markers, which indicates that Barx1-ENGR mis-expression leads to the loss of expression of *Gdf5* and *Atx* in the infected cells of the interzone. However, Barx1-ENGR failed to upregulate *Col2a1* expression in the infected cells and did not convert flattened interzone cells to a rounded morphology (Fig. S5). Therefore, it appears that Barx1 is crucial for interzone formation. However, further experiments are required to assess its exact role.

Development (2023) 150, dev201335. doi:10.1242/dev.201335

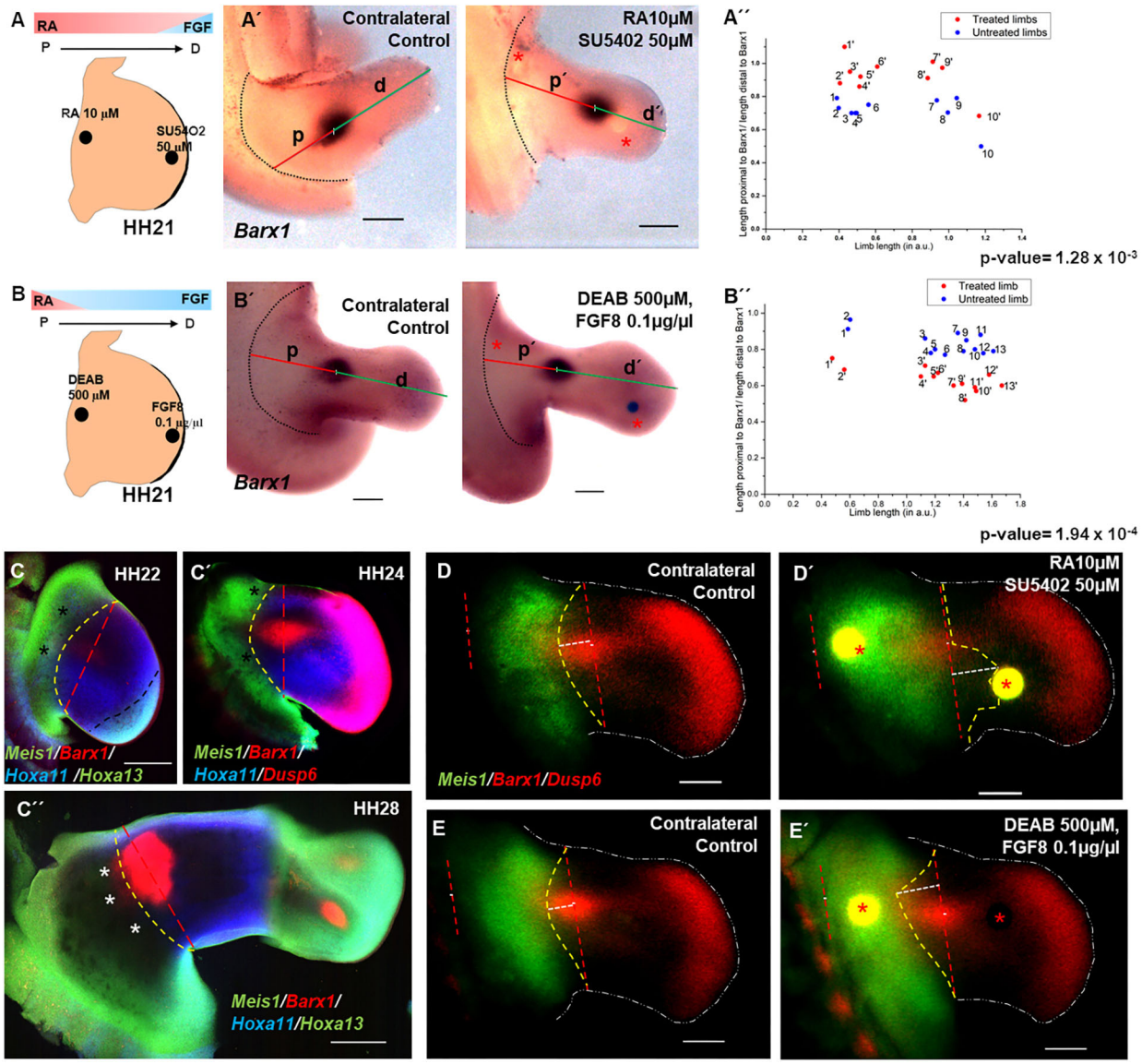

Fig. 4. Simultaneous perturbation of RA and FGF gradients alters segmentation position. (A,B) Bead implantation procedure. (A′,B′) Barx1 detection in HH24-25 chick embryos after implantation of RA- and SU5402-soaked beads (A′), and DEAB- and FGF8 protein-soaked beads (B′) in right hind limb bud at HH21. (A″,B″) Graphs representing the ratio of length proximal and distal to *Barx1* expression (*y*-axis) and total limb length (*x*-axis) from treated (red, ′) and untreated (blue) limbs. Treated and untreated limbs from the same embryo are labelled with the same number. (C-C″) HCR RNA *in situ* hybridization for *Meis1*, *Hoxa11*, *Barx1*, *Hoxa13* and *Dusp6* in developing chick limb bud. Black and white asterisks indicate faint *Hoxa11* and *Meis1* expression, respectively. (D-E′) Non-equivalent shifts in the segmentation marker *Barx1* and the segment marker *Meis1*. Expression of both *Dusp6* (in the distal limb bud) and *Barx1* (in the medial region) are detected in red. (*n*=5 and *n*=4 for the RA- and SU5402-soaked bead, and the DEAB- and FGF8-soaked bead, respectively). Red asterisks indicate the positions of the bead. Dashed red and yellow lines indicate the peak of the *Barx1* expression domain and distal boundary of *Meis1* expression, respectively. The white dashed lines indicate the limb bud boundary. p, p′ and d, d′ represent lengths proximal and distal to *Barx1* expression, respectively. Scale bars: 300 µm.

A shift in the proximal-most interzone site upon simultaneous perturbation of both RA and FGF signaling

We next investigated whether perturbation of RA-FGF signaling gradients resulted in the shift of the *Barx1* expression domain around the time of interzone formation (HH24-25). Following the protocol described above, simultaneous implantation of RA- (10 µM) and SU5402-soaked (50 µM) beads shifted the *Barx1* expression domain distally, i.e. away from the body flank, whereas implanting DEAB- (500 µM) and FGF8-soaked (0.1 µg/µl) beads shifted the *Barx1* expression domain proximally, i.e. closer to the body flank, in HH24-25 treated limbs when compared with their respective contralateral control limb (Fig. 4A-B″). The change in the ratios was observed due to reciprocal changes in the lengths, both proximal and distal to the Barx1 expression domain (Tables S3 and S4). The observed shifts in the *Barx1* expression domain are in line with changes in skeletal element length ratios observed at later developmental stages, and suggest that shifts in the segmentation site upon perturbing RA-FGF signaling gradients at the early stage contribute to altered length ratios observed at later developmental stages.

The relationship between expression of putative segment markers and the segmentation marker Barx1

The question that remains unanswered is how is the joint site specified? Two possibilities exist, which are not necessarily

Development (2023) 150, dev201335. doi:10.1242/dev.201335

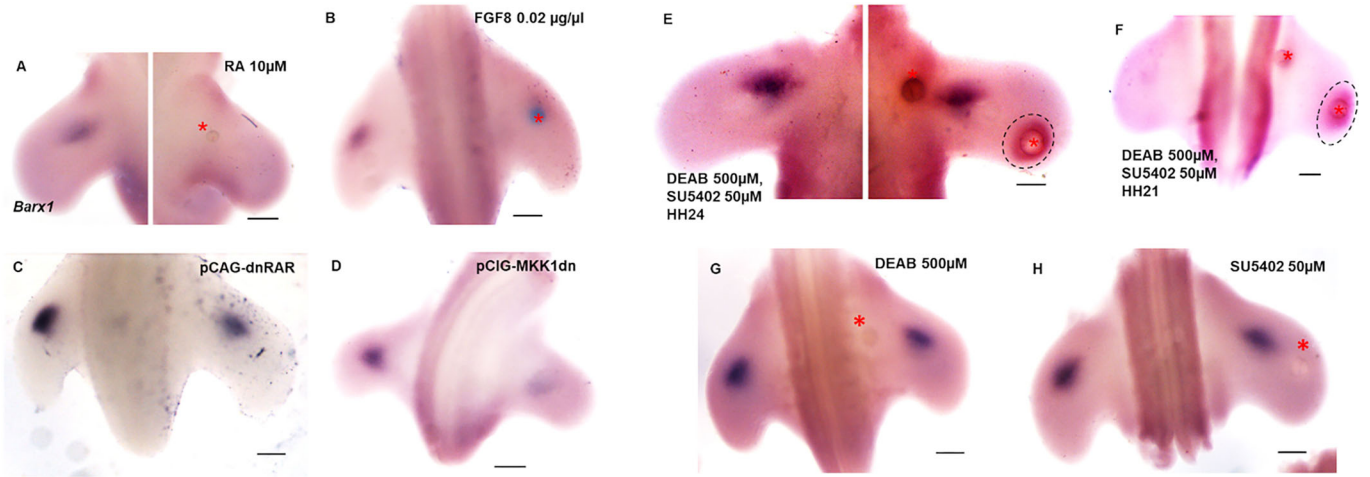

Fig. 5. Simultaneous downregulation of RA and FGF signaling induces ectopic *Barx1* expression. (A-D) Reduced *Barx1* expression in the developing chick limb bud upon increased RA signaling levels (A) (*n*=7), increased FGF signaling levels (B) (*n*=7), decreased RA signaling levels (C) (*n*=4) or decreased FGF signaling (D) levels (*n*=3) at HH23-24. (E) *Barx1* expression 12 h after DEAB- (500 µM) and SU5402-soaked (50 µM) bead implantation in limb flank and distal limb, respectively, at HH24 (*n*=13). (F) *Barx1* detection 6 h after DEAB- (500 µM) and SU5402-soaked (50 µM) bead implantation in limb flank and distal limb, respectively, at HH21 (*n*=5). (G,H) There is no ectopic *Barx1* expression when detected 12 h after DEAB-soaked (500 µM) bead implantation in limb flank (*n*=5) (G) or after SU5402-soaked (50 µM) bead implantation in distal limb at HH23 (*n*=5) (H). Right limb, treated. Red asterisks indicate the positions of beads (AG-1X2 beads in A; Affi-Gel Blue beads in B). Dashed circles indicate ectopic *Barx1* expression. Scale bars: 300 µm.

mutually exclusive: (1) segments are determined first and joints are induced where the segments meet; or (2) joints are determined first and segments are later specified on either side of the joints. In order to investigate these possibilities, we used the third generation *in situ* hybridization chain reaction (Choi et al., 2018), and examined *Barx1* expression with reference to the domains of expression of known putative segment markers *Meis1*, *Hoxa11* and *Hoxa13* (Fig. 4C-C″). At HH24 or earlier, there is no sharp boundary between *Meis1* and *Hoxa11* expression domains. We next investigated the relative expression domains of the putative segment markers and Barx1 in untreated limbs and in limbs where RA-FGF signaling was perturbed. In unperturbed HH22 and HH24 embryonic chick limb bud contexts, the *Barx1* expression domain normally resides immediately adjacent to the distal boundary of *Meis1* expression and within the *Hoxa11* expression domain, while at HH28, the *Barx1* expression domain is at the border of *Meis1* and *Hoxa11* expression domains. Simultaneous implantation of RA- and SU5402-soaked beads at HH20-21 led to the distal expansion of the *Meis1* expression domain, resulting in partial overlap of the *Barx1* and *Meis1* expression domains. In contrast, implantation of DEAB- and FGF8-soaked beads at HH20-21 led to the retraction of *Meis1* expression proximally, resulting in an increase in the gap between *Barx1* and *Meis1* expression domains in HH24 chick limbs (Fig. 4D-E′ and Table S5). The uncoordinated change in relative expression domains of *Meis1* and *Barx1* suggests that the expression of the putative segment markers and the location of interzone induction are not tightly coupled. It appears that initially the expression of putative segment markers and *Barx1* are independently regulated; once the interzone is formed, the *Barx1* expression is confined to the border of *Meis1* and *Hoxa11* expression.

A low threshold of both RA and FGF signaling is required for *Barx1* expression

We observed that the domain of *Barx1* expression relative to the limb field alters depending on the manipulation of RA and FGF signaling gradients. One of the ways that it can happen is if the manipulation results in differential cell proliferation in the proximal and distal regions of the limb bud. To investigate this, RA-FGF signaling gradients were perturbed, as described above, and embryos were harvested 24 h after bead implantation. The number of proliferating cells in the proximal and the distal regions of the limb bud, as judged by phosphohistone 3 immunoreactivity, was analyzed. We observed that perturbing RA-FGF signaling gradients leads to generic increase or decrease in cellular proliferation that is consistent along the proximo-distal axis (Fig. S6 and Table S6).

Finally, we sought to address the question of how RA-FGF reciprocal gradients specify the location of the Barx1 expression domain. In maxillary primordia, FGF signaling positively regulates *Barx1* expression (Barlow et al., 1999; Tucker et al., 1998). However, in the limb bud, *Barx1* is expressed at a distance from both FGF or RA signaling sources, suggesting that, in this context, neither FGF nor RA signaling alone can induce Barx1 expression (Fig. 2A). To investigate the regulation of *Barx1* expression by RA or FGF, we implanted RA- and FGF8-soaked beads individually close to the putative *Barx1* expression site in HH22-23 limbs. We observed that within 6 h of bead implantations, the endogenous domain of *Barx1* expression was abolished, suggesting high activity of either RA or FGF signaling inhibits *Barx1* expression (Fig. 5A,B and Table S7). We produced similar results upon upregulating RA signaling by *in ovo* electroporation of constitutively active RAR or by upregulating FGF signaling by *in ovo* electroporation of RCAS-FGF8 (Fig. S7A,B and Table S7). We next downregulated RA signaling by *in ovo* electroporation of dominant-negative RAR and FGF signaling by *in ovo* electroporation of dominant-negative MAPKK or diffusible FGFR1 (Delfini et al., 2005; Novitch et al., 2003; Sen et al., 2005). We observed that each of these manipulations downregulated *Barx1* expression (Fig. 5C,D and Fig. S7C). We further corroborated this finding, in part, using the mouse model system, where we found that the expression of a Barx family member was abolished in *Meis1/Meis2* double conditional knockout mice (Fig. S7F,F′) (Delgado et al., 2020). Because a high dose of RA or FGF signaling abolishes Barx1 expression and loss of RA or FGF signaling or a RA downstream transcription factor

Development (2023) 150, dev201335. doi:10.1242/dev.201335

(Meis1/2) also abolish Barx1 expression, it appears that the induction of *Barx1* expression requires a specific low threshold level of both RA and FGF signaling. To test this, we attempted to manipulate RA and FGF signal gradients in such a manner that no overlapping domain of RA and FGF signals existed in the developing limb bud. We therefore soaked beads in varying concentrations of DEAB and SU5402, simultaneously implanted them at the sites of their action in HH22-23 limb buds, and then monitored *Barx1* expression after 12 h of treatment. Contrary to our expectation that the absence of signals would abolish *Barx1* expression, we observed that implantation of DEAB- (500 µM) and SU5402-soaked (50 µM) beads not only kept endogenous *Barx1* expression intact, albeit at a lower intensity, but also led to ectopic expression of *Barx1* near the SU5402 source (Fig. 5E,G,H). Furthermore, we observed precocious *Barx1* expression after 6 h of implantation of DEAB- (500 µM) and SU5402-soaked (50 µM) beads in HH20 limb buds (Fig. 5F). For our hypothesis to be true, i.e. that low levels of RA and FGF signaling are required for Barx1 expression, there should be a low level of RA signaling, far from the source of RA, in the distal limb where SU5402-soaked beads are implanted. To investigate this, *in ovo* electroporation of the RA-signaling reporter RARE-AP was performed. We observed that the RA signaling domain extends beyond the first segmentation site and/or the expression domain of Meis1, a known downstream target of RA signaling in developing chick limb bud. Inhibiting the activity of the Raldh2 enzyme by implanting a DEAB-soaked bead reduces the level of RA signaling activity in the distal limb bud (Fig. S8). Taken together, we propose that a narrow range of low concentrations of both RA and FGF signaling is required for Barx1 expression.

When embryos implanted with DEAB- (500 µM) and SU5402-soaked (50 µM) beads at HH22-23 are allowed to develop to later developmental stages, we observed a kink and reduced ossification in the zeugopod at the SU5402-soaked bead implantation site. Such limbs also displayed features of ectopic/expanded interzone formation, as seen by lowered levels of cartilage-specific Safranin-O dye staining, cell-flattening and ectopic expression of *Atx* and *Gdf5* around the SU5402 source (Fig. 6). Even around the endogenous interzone, a kink in the skeletal anlage forms and reduced ossification are observed. These data provide further support that Barx1 expression is sufficient for the induction of interzone-like features.

DISCUSSION

Neither the factor(s) that induces cartilage segmentation in a developing limb-bud nor the molecular mechanisms that dictate the sites of expression of such a factor have been identified to date.

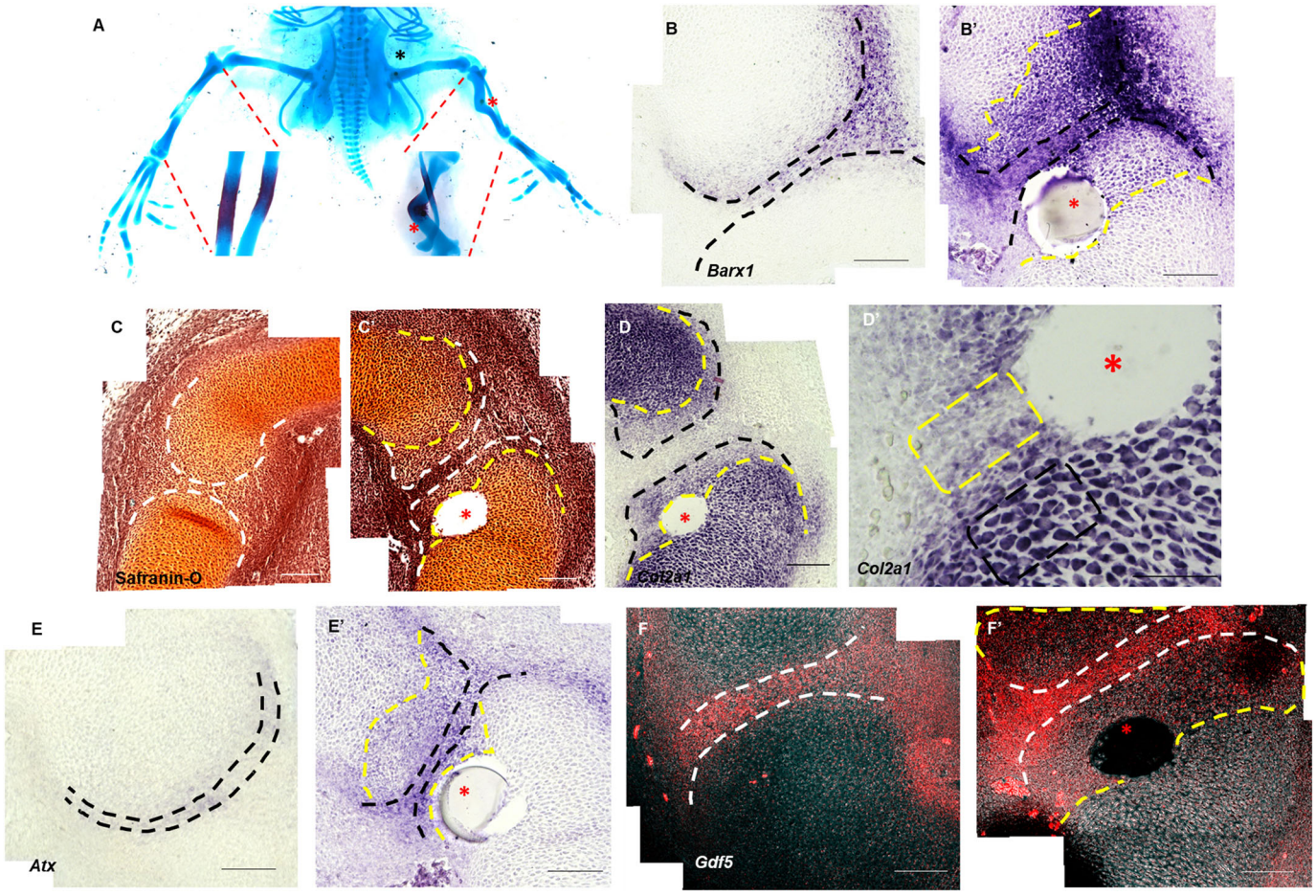

Fig. 6. Simultaneous downregulation of RA and FGF signaling induces an ectopic/expanded domain of joint features in HH30-34 chick limb. (A-F′) Assessment of chick limb after DEAB- (500 µM) and SU5402-soaked (50 µM) bead implantation in skeletal preparations of HH34 chick limbs. (A) Insets show the same specimen after Alizarin Red staining (*n*=4). (B-F′) *Barx1* expression (B,B′), Safranin-O (C,C′), *Col2a1* (D,D′), *Atx* (E,E′) and *Gdf5* expression (F,F′) in HH30 chick limbs (*n*=6). Black asterisk in A indicates the position of a DEAB-soaked bead. Red asterisks indicate the positions of SU5402-soaked beads. Black and white dashed lines mark endogenous expression domains. Yellow dashed lines mark altered expression domains. Dashed yellow and black rectangles in D′ represent *Col2a1*-negative flattened and *Col2a1*-positive round chondrocytes, respectively. Scale bars: 1 mm in A; 100 µm in B-F′.

Development (2023) 150, dev201335. doi:10.1242/dev.201335

Here, we began by considering somitogenesis as a paradigm, and initially arrived at the well-known RA and FGF signaling pairs as candidate factors to investigate further. However, limb segmentation is distinct from somitogenesis. For example, as segmentation of pre-somitic mesoderm occurs in a periodic manner from anterior to posterior, with periodicity being maintained by a known molecular clock involving an intricate network of factors (Jouve et al., 2000; Palmeirim et al., 1997), no detailed clock has been reported in the formation of limb joints (Pascoal et al., 2007). Furthermore, despite several attempts, we could not detect the presence of active Notch signaling during limb cartilage segmentation, which is known to be responsible for pre-somitic mesoderm segmentation (Sato et al., 2002).

Nevertheless, taking hints from molecular networks/gradients involved in the segmentation of pre-somitic mesoderm, we separately individually or simultaneously perturbed the RA or/and FGF signaling gradients across the early limb. Only when we perturbed both signaling pathways simultaneously, e.g. when one is upregulated while the other is downregulated, did we observe significant changes in femur-to-tibia length ratios while keeping the overall limb lengths similar. The absence and presence of changes in skeletal element length ratios upon individual and dual bead implantations, respectively, is possibly due to the action of a known compensatory, mutually antagonistic relationship between these pathways (del Corral et al., 2003; Moreno and Kintner, 2004; Vermot et al., 2005; Yashiro et al., 2004). In previous studies in which only RA or FGF signaling was perturbed, limbs exhibited abnormalities (Mariani et al., 2008; Yashiro et al., 2004). However, perturbing the same signaling pathways by bead implantation, as carried out by us, did not induce limb abnormalities. These differences in phenotypes can be attributed to the duration over which the signaling pathways were perturbed, i.e. permanent for genetic knockout versus transient and short-lived for bead implantation. However, at a very high concentration of RA (i.e. specifically when the beads were placed in the distal end of the limb bud) or SU5402, we did observe limb deformities. We experimented with numerous combinations of RA/FGF agonists/antagonists at different concentrations to arrive at the specific combinations where the manipulations resulted only in shifting of the joints site and no other gross developmental abnormalities.

In this study, we relied on the gene *Barx1* as an early interzone marker. Previously, it has also been reported that in mouse mandible cultures, FGF signaling positively regulates Barx1 expression, and that ectopic activity of Barx1 leads to the transformation of incisors to appear more molar-like (Tucker et al., 1998). Interestingly, in the zebrafish model, genetic manipulation experiments of *barx1* demonstrate that Barx1 represses the formation of the jaw joint and promotes cartilage development in the craniofacial skeleton (Nichols et al., 2013). This observation is further supported by Barx1 knockdown experiments that lead to the upregulations of expression of joint markers such as *Gdf5* and *Chrd* (chordin), and the downregulations of osteochondrogenic markers, such as *Col2a1* and *Runx2a*, and the odontogenic marker *Dlx2b* (Sperber and Dawid, 2008).

Therefore, to investigate the role of Barx1 in joint induction in chick embryonic appendicular skeleton, we took advantage of gain- and loss-of-function studies. Through ectopic upregulation of Barx1 activity, we found ectopic interzone-like structures and ectopic expression of interzone markers. Thus, our data strongly suggest that at least in the developing chick appendicular skeleton, Barx1 is sufficient to induce the interzone. This observation is in stark contrast with observations in the zebrafish craniofacial skeleton. Although the reason for this difference is not immediately understood, it may relate to the different tissue lineages underlying the development of each structure, with the craniofacial skeleton arising from neural crest cells, while the limb skeleton arises from lateral plate mesoderm cells.

Before Barx1, several other molecules, e.g. Gdf5, Wnt9a and Jun, were implicated in interzone induction during limb development. The mice bearing mutation in the Gdf5-coding region exhibited features of brachypodism, i.e. loss of digital joints (Storm and Kingsley, 1999). However, gain-of-function studies for Gdf5, in both chick and mice, did not induce ectopic interzone or joints, but suppressed endogenous joints (Storm and Kingsley, 1999; Tsumaki et al., 2002). Misexpression of Wnt9a, previously known as Wnt14, could induce expression of several interzone markers, such as autotaxin and Gdf5, and downregulate the expression of Col2a1 in the cartilage anlagen (Hartmann and Tabin, 2001). However, the chondrocytes affected by Wnt9a misexpression did not exhibit the characteristic flattened morphology of the interzone cells. A subsequent study where Wnt9a activity was depleted demonstrated no major effect on interzone initiation and/or joint morphogenesis (Später et al., 2006). Jun, a transcription factor belonging to the AP1 family, is expressed in an interzone-restricted manner. The loss of limb-specific Jun activity led to upregulated Col2a1 expression and downregulation of the interzone marker Gdf5. However, the interzone was specified normally in the *Jun* mutant mice. Joint development was largely normal, albeit with some defects (Kan and Tabin, 2013). Therefore, none of the genes described in the literature so far to have interzone-specific expression seem to be important for interzone induction per se. Barx1 is the first molecule identified that induces all the features of an interzone. However, misexpression of Barx1 does not lead to ectopic joint formation. Joint morphogenesis requires movement of the adjacent skeletal elements around each other, which in turn requires the involvement of muscles and appropriate attachment of tendons/ligaments, etc. (Rolfe et al., 2014; Singh et al., 2018). It is unlikely that Barx1 can induce appropriate patterning of the muscles and attachment of tendons/ligaments at the site of an ectopic interzone, leading to the morphogenesis of a fully functional joint.

Next, although we could not knock down or knock out Barx1 in chick or mouse, due to technical limitations, we were able to inhibit Barx1 function in the limb using a dominant-negative Barx1-EnR construct. Misexpression of this construct blocked the expression of joint markers such as *Atx* and *Gdf5*, but could not induce a reversal of cell shape (from flattened to round) or upregulate *Col2a1*. It is possible that by the time Barx1-EnR infection was established in limb mesenchymal cells, interzone specification had already occurred and the Barx1-EnR fusion protein could only block further joint differentiation.

There is a second possibility. As demonstrated, full-length Barx1 does not elicit the full range of phenotypes of interzone induction, but Barx1-VP16 does, suggesting that Barx1 needs other collaborating partners. On the other hand, Barx1-Enr blocks some of the features of interzone but not all, suggesting that there is functional redundancy with other proteins, possibly Barx2. As joint morphogenesis is a key feature for vertebrate development, it is likely that there are several layers of redundancy built in the program. Barx1 is certainly a key player but it appears that there are other molecules that play a key role in induction of joint site. Unfortunately, existing literature on Barx1 or Barx2 loss of function in mice does not shed any light on the necessity of Barx proteins in joint induction: Homozygous *Barx1*-null embryos survive only until E13 but are largely normal compared with wild-type littermates of the same stage (Kim et al., 2005); *Barx2*-null mice,

Development (2023) 150, dev201335. doi:10.1242/dev.201335

which survive until adulthood, also lack any obvious joint phenotype (Olson et al., 2005). It is possible that a conditional mutant of Barx1 or a Barx1/Barx2 double mutant, driven by an early limb mesenchyme-specific Cre such as Prx1-Cre or Dermo1-Cre, could result in establishing the necessity of Barx proteins in interzone/joint induction.

In chick, whereas Barx1 is expressed in a joint-specific manner, Barx2 is expressed in a graded manner near the FGF signaling source, during early developmental stages. Conversely, in mice, whereas Barx2 is expressed in a joint-specific manner, Barx1 is expressed in a graded manner near the FGF signaling source, during early developmental stages (Fig. S7). Therefore, it is possible that there is role-reversal in the functions of Barx1 and Barx2 in chick and mouse, as has been seen for other gene orthologs between chick and mouse (Nieto, 2018).

In the chick system, the expression domain of *Barx1* is farthest from both RA and FGF signaling centers, yet both gain-of and loss-of-function of either RA or FGF signaling abolish Barx1 expression. Therefore, it appears that a critical, yet low, threshold of both these signals is required for *Barx1* expression. In this context, it should be noted that implantation of a DEAB-soaked bead in the proximal end of the limb, along with implantation of a SU5402-soaked bead in the distal end of the limb, resulted in the induction of ectopic *Barx1* expression around the SU5402-soaked bead site, and the consequent differentiation of an ectopic interzone. Co-electroporation of a RARE-AP reporter construct along with pCAG-mCherry demonstrated that RA signaling extends close to the distal end. It is likely that, due to DEAB-soaked bead implantation, the RA signaling front receded proximally; with the simultaneous downregulation of FGF signaling, another zone was created that had optimum concentrations of both RA and FGF signaling, which led to ectopic *Barx1* expression.

Analysis of putative enhancers (5 kb upstream) of chick *Barx1* and *Barx2*, as well as mouse *Barx1* and *Barx2* revealed a closely spaced cluster of Meis1- and Fos-Jun (AP1)-binding sites (Fig. S9). Meis1 is a transcription factor acting downstream of the RA signaling, and AP1 is downstream of FGF signaling (Kim et al., 1998; Mercader et al., 2000). This supports our hypothesis that both RA and FGF signaling are required for Barx gene expression in chick and mouse. However, what remains unclear is why and how chick *Barx1* and mouse *Barx2* are expressed in joint-specific manners while chick *Barx2* and mouse *Barx1* are not. Expression of *Barx2* in mouse is abolished in the absence of *Meis1* and/or *Meis2*, suggesting that Meis genes are involved in the induction of Barx genes. However, in chick, at an early stage, HH22-24, Meis1 expression does not overlap the Barx1 domain (Fig. 4C,C′). ChIP-Seq analysis with Meis1, Meis2 and AP1, in both species, will be needed to gain further clarity.

Another molecular framework that we could have investigated would have been to test a hypothesis that the border between putative segment markers acts as a molecular organizer for the induction of joint sites. To this end, our observations suggest that the initial domains of expression of the putative segment markers do not precisely mark the future segments. This observation is in keeping with lineage tracing data reported earlier (Delgado et al., 2020; Sato et al., 2007). Yet we note that, at later embryonic stages, the expression of Barx1 does reside at the border of Meis1 and Hoxa11. Our data, taken together with existing literature, suggest that RA-FGF reciprocal gradients are involved in initiating the expression of the putative segment markers, as well as specifying the location of expression of the segmentation gene *Barx1*. Subsequently, once Barx1 induces the interzone, the expression domains of putative segment markers become restricted to the segments without any overlap and Barx1 continues to be expressed at the border.

Our data suggest that the expression of *Barx1* and/or *Barx2* and the putative segment markers is not tightly coupled. There may be several reasons for this. One possibility is that the threshold requirement of RA and/or FGF signaling for *Meis1*, *Meis2*, *Hoxa11*, *Hoxa13* and *Barx1/2* is different from each other. There is some evidence in the literature to support such a speculation. For example, RA can induce expression of *Meis1* over a broad range of concentrations. On the other hand, FGF signaling inhibits *Meis1* expression only when the level of RA signaling is low (Capdevila et al., 1999; Mercader et al., 2000). The regulation of *Hoxa11* expression by RA signaling appears to be position dependent, i.e. RA inhibits *Hoxa11* expression at its proximal border, whereas it promotes *Hoxa11* expression at its distal border (Tabin and Wolpert, 2007). Furthermore, it has been speculated that the expression of *Hoxa11* is independent of FGF signaling (Hashimoto et al., 1999; Vargesson et al., 2001). RA signaling inhibits *Hoxa13* expression, whereas FGF signaling stimulates its expression (Hashimoto et al., 1999; Vargesson et al., 2001). Our experimental studies suggest that the expression of *Barx1* requires a narrow range of low signaling levels of both RA and FGF. Additionally, Meis1 and/or Meis2 regulates the domain of *Hoxa11* and *Hoxa13*. However, this regulation is not direct (Delgado et al., 2020). Therefore, the possibility exists that a distinct set of transcriptional regulators, in conjunction with downstream effectors of RA and/or FGF signaling are needed for the expression of *Meis1*, *Meis2*, *Hoxa11*, *Hoxa13*, *Barx1* and *Barx2*, which in turn leads to de-coupling of expression of these genes.

Although the present study is limited to the specification of only the first joint, it is possible that the positioning of subsequently more distal joints of the limb might also be dictated by the interplay of RA and FGF signaling pathways. Newly formed joints express *Raldh2* and may in turn act as new RA sources, similar to newly formed somites during somitogenesis (Dubrulle and Pourquié, 2004) (Fig. S10). As skeletal element lengths and their ratios are crucial parameters in affording appropriate mechanical advantages to species to meet locomotion and feeding needs across their life span (Schultz, 1944; Smith and Savage, 1956), our studies additionally posit that the doses of RA and FGF signaling must be subjected to strong evolutionary pressure in and across species. In future studies, this hypothesis should be tested.

MATERIALS AND METHODS

Tissues

Fertilized White Leghorn Chicken eggs were obtained from the Central Avian Research Institute of India (Bareilly, UP, India), from Chandra Shekhar Azad Agricultural University (Kanpur, UP, India) and from Ganesh Enterprises (Nankari, Kanpur, UP, India). Eggs were incubated at 38°C in a humidified chamber to be treated and/or harvested at specific stages of development, as assessed by Hamburger and Hamilton staging criteria (Hamburger and Hamilton, 1951).

Meis1/Meis2 double conditional knockout mice were generated by recombining *Meis1* and *Meis2* floxed alleles with $Dll1^{Cre}$, as previously described (Delgado et al., 2020). Mice were handled in accordance with Centro Nacional de Investigaciones Cardiovasculares (CNIC) Ethics Committee, Spanish laws and the European Union (EU) Directive 2010/63/EU for the use of animals in research. All mouse experiments were approved by the CNIC and Universidad Autónoma de Madrid Committees for 'Ética y Biene-star Animal' and the area of 'Protección Animal' of the Community of Madrid with reference PROEX 220/15.

Tissue processing, embedding and sectioning

Embryos were harvested in phosphate-buffered saline (PBS), hindlimbs were dissected and fixed overnight at 4°C in 4% paraformaldehyde (PFA) in PBS. Post-fixation the tissues were washed in PBS twice for 5 min each and then dehydrated to 100% ethanol via an ethanol gradient from 25% ethanol

Development (2023) 150, dev201335. doi:10.1242/dev.201335

in PBS to 50% ethanol in PBS to 75% ethanol in water with 5 min incubation in each. The tissues were then dehydrated in 100% ethanol twice for 10 min each and then cleared in xylene. Next, the tissues were treated with 1:1 solution of xylene:paraffin wax for 20 min at 65°C and then kept in 100% paraffin wax at 65°C for 1 h, followed by treatment in 100% paraffin wax at 65°C for 8-9 h. The tissues were then embedded in fresh paraffin wax and kept at 4°C. Paraffin wax-embedded limbs were sectioned along the para-sagittal plane using microtome to obtain 5 µm sections on poly-L-lysine coated glass slides.

Paraffin wax section processing before histology, immunohistochemistry or RNA *in situ* hybridization

Paraffin wax-embedded tissue sections were initially baked on hot plate at 60°C for 1 h, followed by dewaxing in xylene three times for 5 min each. The sections were next treated with 100% ethanol twice for 5 min each and then rehydrated to PBS via an ethanol gradient from 75% ethanol to 50% ethanol to 25% ethanol for 5 min each.

Skeletal preparations and length measurements

The embryos were harvested and eviscerated in PBS and fixed in 95% ethanol for at least 2-3 days followed by an overnight fixation in 100% acetone. Next, the tissues were stained for 2-3 days with a mixture of one volume of 0.3% Alcian Blue solution in 95% ethanol:one volume of 0.1% Alizarin Red solution in 70% ethanol:one volume of glacial acetic acid:17 volumes of 70% ethanol. Post-staining, the tissues were cleared in 1% potassium hydroxide and photographed under a dissection microscope. Limbs were dissected out from the skeleton preparations and were carefully imaged from the same angle to avoid any foreshortening. The skeletal element lengths were measured by ImageJ software using Straight line tool. The skeletal element lengths were measured along their two ends. Femur-to-tibia length ratios were determined for both treated and contralateral control limb, and statistical significance of variation in length ratios was determined using a paired Student's *t*-test (two-tailed) method.

Section RNA *in situ* hybridization

cDNA clones used to make digoxigenin-labeled antisense riboprobes generated by *in vitro* transcription are: *Atx* (ChEST 520a5), *Barx1* (ChEST 52p17), *Col2a1* (ChEST 197l15) and *Raldh2* (564a12). The cDNA clones for FGF8 and Cyp26b1 were generated by cloning in pBS and TA backbones, respectively. RNA *in situ* hybridization was performed as described previously for chick (Singh et al., 2017).

Whole-mount RNA *in situ* hybridization and measurements

cDNA clones used to make digoxigenin-labelled antisense riboprobes generated by *in vitro* transcription are same as discussed above. Whole-mount *in situ* hybridization experiments were performed as per the protocol of Wilkinson and Nieto (1993). Limbs were dissected out and were carefully imaged from the same angle to avoid any foreshortening. Approximate center of *Barx1* expression was determined as the point of highest *Barx1* signal intensity. A line joining the point of the distal-most extremity of limb bud and approximate center of *Barx1* expression was drawn and extended to the body flank. The lengths proximal and distal to *Barx1* expression were measured using ImageJ software using Straight line tool. Ratio of lengths proximal and distal to *Barx1* expression were determined for both treated and contralateral control limb, and the statistical significance of variation in length ratios was determined using a paired Student's *t*-test (two-tailed).

Third generation *in situ* hybridization chain reaction (HCR) experiments

HCR probe sets and HCR amplifiers tagged with Alexa Fluor 488 against *Meis1* and *Hoxa13*, with Alexa Fluor 546 against *Hoxa11*, with Alexa Fluor 594 against *Barx1* and *Dusp6*, and with Alexa Fluor 647 against *Gdf5* were commercially synthesized by Molecular Instruments. The chick tissues were cleared using the CUBIC method (Gómez-Gaviro et al., 2017) and HCR *in situ* hybridization was performed as described previously for chick (Choi et al., 2018). Images were acquired using Leica Stellaris 5 (Fig. 4C-C′′) or Leica MZ10F (Fig. 4D-E′).

Fig. 4D-E′ images had background fluorescence. Therefore, an intensity threshold of 30 for Fig. 4D,D′ and 50 for Fig. 4E,E′ for the signal in green (i.e. for *Meis1* expression) was set using ImageJ software. A yellow line was drawn approximately tracing the domain with signal intensity above the set threshold. Points of maximum *Barx1* expression intensity (using ImageJ software) and the proximal-most tip of the limb bud were marked (as white spots). A line passing through the point of maximum *Barx1* expression intensity and approximately parallel to the tangent to proximal limb curvature at the proximal-most point was drawn (marked as red lines). A line perpendicular to the red line and joining the farthest point of the *Meis1* expression domain was drawn (marked as white dotted line) to determine the expansion or regression of the *Meis1* expression domain. The length of this line was determined using ImageJ software. Distances proximal and distal with respect to the Barx1 expression domain were represented with negative and positive values, respectively.

Histology: Safranin-O staining

Safranin-O staining was carried out on de-paraffinized rehydrated sections that were counterstained in Hematoxylin and Fast Green, rinsed in acetic acid and stained with Safranin-O (0.1% in water). Sections were subsequently dehydrated and mounted in DPX Mountant (ThermoFisher Scientific, 18404).

Quantification of *Barx1* expression intensity

The bright-field images were converted to black and white images, followed by inversion to greyscale images using ImageJ software. An oval-shaped selection of the same-sized area was used for both the control and treated limbs to measure *Barx1* mean signal intensity. The statistical significance was determined using a paired Student's *t*-test (two-tailed).

In ovo electroporation

The constructs, RCAS-Barx1 (1 µg/µl), RCAS-Barx1-VP16 (1 µg/µl), RCAS-Barx1-ENR (0.9 µg/µl), pCAG-dnRAR (1.5 µg/µl), pCAG-caRAR (1.5 µg/µl), pCIG-MKKdn (1.5 µg/µl), pSV1-dFGFR1 (1.5 µg/µl), RCAS-FGF8 (1.5 µg/µl), pGL3-RARE-AP (2 µg/µl), Hsp68-R37-LacZ (2 µg/µl) and Hsp68-R37 Mut4-LacZ (2 µg/µl) were combined with 0.5 µg/µl pCAGGS-mCherry and 1% Fast Green injected between the somatic LPM and splanchnic LPM using a microinjector. The embryos were initially lowered by removing 2-3 ml of albumin and a window was made to visualize the embryo under the vitelline membrane. This vitelline membrane was shorn near the hindlimb field and bathed in 100 µl of a sterile PBS+pen strep solution (ThermoFisher Scienific, 10378016). At stage HH14, the DNA and Fast Green dye mix was injected into the embryonic space between the somatic LPM and splanchnic LPM at a concentration of 2 µg/µl using a microinjector. As soon as the DNA was injected, a platinum cathode was placed within the albumin beneath the yolk sac while an L-shaped anode was placed in parallel to the embryo over the hindlimb field before electric pulses (10 V, 50 ms pulse-on, 950 ms pulse-off, five repetitions) were applied. Care was taken that the electrodes did not touch the embryo when the electric field was applied.

Counting of proliferating cells

Simultaneous implantation of a RA-soaked bead (10 µM) in the proximal end and a SU5402-soaked bead (50 µM) in the distal end, or a DEAB-soaked bead (500 µM) in the proximal end and FGF8-soaked bead (0.1 µg/µl) in the distal end of HH20-21 chick hind limb buds was performed and the embryos were harvested 24 h after bead implantation i.e. at HH24-25. The limbs were embedded in paraffin wax and sectioned at 12 µm. Subsequently, immunohistochemistry for phosphohistone H3 (pH3) (Sigma, H0412), a mitotic marker, was carried out (as described by Singh et al., 2017). The numbers of pH3-positive cells were counted for the contralateral control limbs as well as the treated limbs. Equal number of sections (six for HH24 limbs, four for HH24-25 or HH25 limbs) from contralateral and treated limbs were analyzed to count pH3-positive cells. A line joining the distal-most tip of the limb bud and an approximate mid-point of proximal flank was drawn. The limb-field was split into proximal and distal halves by drawing another line parallel to the proximal flank and passing through the mid-point of the previously drawn line.

Development (2023) 150, dev201335. doi:10.1242/dev.201335

Construct generation

The avian retroviral vector RCASBP(A) was used to deliver constitutively active (cBarx1-VP16), full-length (cBarx1) and dominant-negative (cBarx1-ENGR) versions of chicken Barx1 (cBarx1), and were named as RCASBP(A)-cBarx1-VP16, RCASBP(A)-cBarx1 and RCASBP(A)-cBarx1-ENGR, respectively. Chicken Barx1 ORF was chemically synthesized and procured from GenScript cloned as pUC57-cBarx1 and thereafter subcloned into a RCAS vector.

Bead implantation

AG1-X2 ion exchange resin beads (150-200 µm diameter; BioRad) were soaked for 45 min in retinoic acid (Sigma, R2625)/Diethylaminobenzaldehyde (DEAB, Sigma, D86256)/SU5402 (Tocris, 3300) dissolved in DMSO, achieving mentioned dilutions. Beads were briefly stained in Fast Green and rinsed three times in saline solution. Bead insertion was performed close to the body flank or most distal border of the AER in chick limbs at stages indicated. Control beads were incubated in DMSO alone and treated as described above with RA, DEAB or SU5402. Affi-gel blue beads (BioRad) were rinsed in phosphate-buffered saline three times for 10 min and incubated (room temperature, 1 h) with recombinant FGF8b (R&D Systems) at the indicated dilutions on a culture dish. Control beads were incubated in PBS alone and treated as described above for FGF8b. For bead experiments involving simultaneous perturbation of RA and FGF signaling gradients, the concentrations of RA, SU5402, DEAB and FGF8 were serially titrated down such that resulting limbs form without any gross morphological defects.

3C2 staining

The sections were deparaffinized, rehydrated in PBS via an ethanol gradient as described above, followed by post-fixation in 4% PFA for 5 min. Sections were then washed in PBT for 5 min three times. For detecting RCAS-infected cells, sections were preblocked with MST for 30 min before incubating with anti-GAG 3C2 antibody (AMV-3C2 from DHSB) at 1:5 dilution in MST for overnight at 4°C. Immunofluorescence was detected using the secondary antibody Alexa Fluor 488 conjugated anti-mouse IgG (1:200; Jackson Immunoresearch Laboratories, 115-545-003). The tissues were counterstained with DAPI and mounted in Vectashield antifade reagent (Vector Laboratories; H-1000).

β-Galactosidase staining

Embryos with the Gdf5-LacZ reporter (Chen et al., 2016) electroporated were fixed for 45 min in fresh 4% PFA in PBS at room temperature, followed by washing three times in wash buffer, containing 2 ml 1 M $MgCl_2$,10 ml 1% deoxycholate, 2 ml 10% NP40 and 988 ml 0.1 M sodium phosphate (pH 7.3). Embryos were stained in X-Gal staining buffer (1 mg/ml) in the dark at room temperature until signal developed. After staining, embryos were briefly washed in wash buffer, post-fixed in 4% PFA for 2 h and imaged under stereomicroscope.

In silico analysis of transcription factor-binding sites

In silico transcription factor-binding site analysis for the transcription factors AP1 and MEIS1 has been performed using ConTra v3 in the 5 kb promoter region from the transcription start site of the BARX1 and BARX2 genes with Mouse (*Mus musculus*) and chicken (*Gallus gallus*) as reference organisms. For this analysis, a core stringency of 0.95 and a similarity stringency of 0.85 were used. For MEIS1 transcription factor, the position weight matrices V$MEIS1_02, M01419, V$MEIS1_01, M00419, MA0498.2 and MA0498.2 were considered; for the AP1 transcription factor, position weight matrices MA0940.1, MA0940.1, V$AP1_01, M00517, V$AP1_Q2_01, M00924, V$AP1_Q6_01, M00925, V$AP1_Q4_01, M00926, V$AP1_C,M00199, V$AP1_Q4,M00188, V$AP1FJ_Q2, M00172, V$AP1_Q2,M00173 and V$AP1_Q6,M00174 were considered. We used stringencies of 0.95 for both the core and similarity matrix matches (matrix score) for schematic representation of transcription binding sites.

Acknowledgements

We thank Olivier Pourquié for generously providing pCIG-MKK1dn and pSV1-diffusible FGFR constructs, Cliff Tabin for providing the pGEMT-Gdf5, pBS-Meis1 construct, Vikas Trivedi for guidance in designing HCR probes, and Pradip Sinha for the Leica Stellaris 5 confocal microscope facility. We thank Debojyoti Chakraborty, Riya Rauthan, Jyoti Tripathi and Mahima Bharti for providing assistance in imaging HCR probe-stained whole embryos. We also thank Cliff Tabin and Jonaki Sen for helpful discussions.

Competing interests

The authors declare no competing or financial interests.

Author contributions

Conceptualization: A.B., U.S.Y., T.B., P.N.S.; Methodology: A.B., U.S.Y., T.B., P.N.S., P.G., S.C., I.D., H.Z., T.D.C., M.T.; Validation: A.B., U.S.Y., T.B., P.N.S.; Formal analysis: U.S.Y., T.B., P.N.S.; Investigation: A.B., U.S.Y., T.B., P.N.S., P.G., S.C., I.D., H.Z., M.T.; Resources: A.B., T.D.C, M.T.; Data curation: U.S.Y., T.B., P.N.S.; Writing - original draft: A.B., U.S.Y., T.B., P.N.S., T.D.C.; Writing - review & editing: A.B., U.S.Y., T.B., T.D.C; Visualization: A.B., U.S.Y., T.B., P.N.S.; Supervision: A.B.; Project administration: A.B.; Funding acquisition: A.B., T.D.C., M.T.

Funding

This work was supported by grants from the Department of Biotechnology, Ministry of Science and Technology, India (BT/PR27714/BRB/10/1649/2019, BT/PR11202/MED/32/46/2008 and BT/IN/DENMARK/02/PDN/2011 to A.B.), by a grant from the National Institutes of Health National Institute of Arthritis and Musculoskeletal and Skin Diseases (R01AR070139-01A1 to T.D.C.), by a grant from the Science and Engineering Research Board, Ministry of Science and Technology, India (CRG/2020/001313), and by a grant from the Ministerio de Ciencia e Innovación (PGC2018-096486-B-I00 to M.T.). Deposited in PMC for release after 12 months.

Data availability

All data are available in the main text or the supplementary materials.

Peer review history

The peer review history is available online at https://journals.biologists.com/dev/lookup/doi/10.1242/dev.201335.reviewer-comments.pdf.

References

Barlow, A. J., Bogardi, J.-P., Ladher, R. and Francis-West, P. H. (1999). Expression of chick Barx-1 and its differential regulation by FGF-8 and BMP signaling in the maxillary primordia. *Dev. Dyn.* **214**, 291-302. doi:10.1002/(SICI)1097-0177(199904)214:4<291::AID-AJA2>3.0.CO;2-E

Boulet, A. M. and Capecchi, M. R. (2004). Multiple roles of Hoxa11 and Hoxd11 in the formation of the mammalian forelimb zeugopod. *Development (Cambridge, England)* **131**, 299-309. doi:10.1242/dev.00936

Capdevila, J., Tsuki, T., Esteban, C. R., Zappavigna, V. and Belmonte, J. C. I. (1999). Control of vertebrate limb outgrowth by the proximal factor Meis2 and distal antagonism of BMPs by Gremlin. *Mol. Cell* **4**, 839-849. doi:10.1016/S1097-2765(00)80393-7

Chen, H., Capellini, T. D., Schoor, M., Mortlock, D. P., Reddi, A. H. and Kingsley, D. M. (2016). Heads, shoulders, elbows, knees, and toes: modular Gdf5 enhancers control different joints in the vertebrate skeleton. *PLoS Genet.* **12**, e1006454. doi:10.1371/journal.pgen.1006454

Choi, H. M. T., Schwarzkopf, M., Fornace, M. E., Acharya, A., Artavanis, G., Stegmaier, J., Cunha, A. and Pierce, N. A. (2018). Third-generation in situ hybridization chain reaction: Multiplexed, quantitative, sensitive, versatile, robust. *Development (Cambridge, England)* **145**, dev165753. doi:10.1242/dev.165753

Cong, L., Ran, F. A., Cox, D., Lin, S., Barretto, R., Habib, N., Hsu, P. D., Wu, X., Jiang, W., Marraffini, L. A. et al. (2013). Multiplex genome engineering using CRISPR/Cas systems. *Science (New York, N.Y.)* **339**, 819-823. doi:10.1126/science.1231143

Cooper, K. L., Oh, S., Sung, Y., Dasari, R. R., Kirschner, M. W. and Tabin, C. J. (2013). Multiple phases of chondrocyte enlargement underlie differences in skeletal proportions. *Nature* **495**, 375-378. doi:10.1038/nature11940

del Corral, R. D., Olivera-Martinez, I., Goriely, A., Gale, E., Maden, M. and Storey, K. (2003). Opposing FGF and retinoid pathways control ventral neural pattern, neuronal differentiation, and segmentation during body axis extension. *Neuron* **40**, 65-79. doi:10.1016/S0896-6273(03)00565-8

Delfini, M.-C., Dubrulle, J., Malapert, P., Chal, J. and Pourquié, O. (2005). Control of the segmentation process by graded MAPK/ERK activation in the chick embryo. *Proc. Natl Acad. Sci. USA* **102**, 11343-11348. doi:10.1073/pnas.0502933102

Delgado, I., López-Delgado, A. C., Roselló-Díez, A., Giovinazzo, G., Cadenas, V., Fernández-De-Manuel, L., Sánchez-Cabo, F., Anderson, M. J., Lewandoski, M. and Torres, M. (2020). Proximo-distal positional information encoded by an Fgf-regulated gradient of homeodomain transcription factors in the vertebrate limb. *Sci. Adv.* **6**, eaaz0742. doi:10.1126/sciadv.aaz0742

Dubrulle, J. and Pourquié, O. (2004). Coupling segmentation to axis formation. *Development* **131**, 5783-5793. doi:10.1242/dev.01519
Fell, H. B. and Canti, R. G. (1934). Experiments on the development *in vitro* of the avian knee-joint. *Proc. R. Soc. Lond. Ser. B Biol. Sci.* **116**, 316-351. doi:10.1098/rspb.1934.0076
Fromental-Ramain, C., Warot, X., Messadecq, N., Lemeur, M., Dollé, P. and Chambon, P. (1996). Hoxa-13 and Hoxd-13 play a crucial role in the patterning of the limb autopod. *Development (Cambridge, England)* **122**, 2997-3011. doi:10.1242/dev.122.10.2997
Galloway, J. L., Delgado, I., Ros, M. A. and Tabin, C. J. (2009). A reevaluation of X-irradiation-induced phocomelia and proximodistal limb patterning. *Nature* **460**, 400-404. doi:10.1038/nature08117
Gómez-Gaviro, M. V., Balaban, E., Bocancea, D., Lorrio, M. T., Pompeiano, M., Desco, M., Ripoll, J. and Vaquero, J. J. (2017). Optimized CUBIC protocol for 3D imaging of chicken embryos at single-cell resolution. *Development* **144**, 2092-2097. doi:10.1242/dev.145805
Hamburger, V. and Hamilton, H. L. (1951). A series of normal stages in the development of the chick embryo. *J. Morphol.* **88**, 49-92. doi:10.1002/jmor.1050880104
Hartmann, C. and Tabin, C. J. (2001). Wnt-14 plays a pivotal role in inducing synovial joint formation in the developing appendicular skeleton. *Cell* **104**, 341-351. doi:10.1016/S0092-8674(01)00222-7
Hashimoto, K., Yokouchi, Y., Yamamoto, M and Kuroiwa, A. (1999). Distinct signaling molecules control Hoxa-11 and Hoxa-13 expression in the muscle precursor and mesenchyme of the chick limb bud. *Development* **26**, 2771-2783. doi:10.1242/dev.126.12.2771
Holder, N. (1977). An experimental investigation into the early development of the chick elbow joint. *J. Embryol. Exp. Morphol.* **39**, 115-127. doi:10.1242/dev.39.1.115
Jouve, C., Palmeirim, I., Henrique, D., Beckers, J., Gossler, A., Ish-Horowicz, D. and Pourquié, O. (2000). Notch signalling is required for cyclic expression of the hairy-like gene HES1 in the presomitic mesoderm. *Development (Cambridge, England)* **127**, 1421-1429. doi:10.1242/dev.127.7.1421
Kamei, C. N., Kempf, H., Yelin, R., Daoud, G., James, R. G., Lassar, A. B., Tabin, C. J. and Schultheiss, T. M. (2011). Promotion of avian endothelial cell differentiation by GATA transcription factors. *Dev. Biol.* **353**, 29-37. doi:10.1016/j.ydbio.2011.02.016
Kan, A. and Tabin, C. J. (2013). C-Jun is required for the specification of joint cell fates. *Genes Dev.* **27**, 514-524. doi:10.1101/gad.209239.112
Kim, J., Lin, J.-J., Xu, R.-H. and Kung, H.-F. (1998). Mesoderm induction by heterodimeric AP-1 (c-Jun and c-Fos) and its involvement in mesoderm formation through the embryonic fibroblast growth factor/Xbra autocatalytic loop during the early development of Xenopus embryos. *J. Biol. Chem.* **273**, 1542-1550. doi:10.1074/jbc.273.3.1542
Kim, B.-M., Buchner, G., Miletich, I., Sharpe, P. T. and Shivdasani, R. A. (2005). The stomach mesenchymal transcription factor Barx1 specifies gastric epithelial identity through inhibition of transient Wnt signaling. *Dev. Cell* **8**, 611-622. doi:10.1016/j.devcel.2005.01.015
Kumar, Y., Biswas, T., Thacker, G., Kanaujiya, J. K., Kumar, S., Shukla, A., Khan, K., Sanyal, S., Chattopadhyay, N., Bandyopadhyay, A. et al. (2018). BMP signaling-driven osteogenesis is critically dependent on Prdx-1 expression-mediated maintenance of chondrocyte prehypetrophy. *Free Radic. Biol. Med.* **118**, 1-12. doi:10.1016/j.freeradbiomed.2018.02.016
Logan, M. and Tabin, C. (1998). Targeted gene misexpression in chick limb buds using avian replication-competent retroviruses. *Methods (San Diego, Calif.)* **14**, 407-420. doi:10.1006/meth.1998.0595
Mariani, F. V., Ahn, C. P. and Martin, G. R. (2008). Genetic evidence that FGFs have an instructive role in limb proximal-distal patterning. *Nature* **453**, 401-405. doi:10.1038/nature06876
Mercader, N., Leonardo, E., Azpiazu, N., Serrano, A., Morata, G., Martínez-A, C. and Torres, M. (1999). Conserved regulation of proximodistal limb axis development by Meis1/Hth. *Nature* **402**, 425-429. doi:10.1038/46580
Mercader, N., Leonardo, E., Piedra, M. E., Martinez-A, C., Ros, M. A. and Torres, M. (2000). Opposing RA and FGF signals control proximodistal vertebrate limb development through regulation of Meis genes. *Development* **127**, 3961-3970. doi:10.1242/dev.127.18.3961
Milán, M. and Cohen, S. M. (2000). Subdividing cell populations in the developing limbs of Drosophila: do wing veins and leg segments define units of growth control? *Dev. Biol.* **217**, 1-9. doi:10.1006/dbio.1999.9493
Mohammadi, M., Mcmahon, G., Sun, L., Tang, C., Hirth, P., Yeh, B. K., Hubbard, S. R. and Schlessinger, J. (1997). Structures of the tyrosine kinase domain of fibroblast growth factor receptor in complex with inhibitors. *Science* **276**, 955-960. doi:10.1126/science.276.5314.955
Moreno, T. A. and Kintner, C. (2004). Regulation of segmental patterning by retinoic acid signaling during Xenopus somitogenesis. *Dev. Cell* **6**, 205-218. doi:10.1016/S1534-5807(04)00026-7
Nelson, C. E., Morgan, B. A., Burke, A. C., Laufer, E., Dimambro, E., Murtaugh, L. C., Gonzales, E., Tessarollo, L., Parada, L. F. and Tabin, C. (1996). Analysis of Hox gene expression in the chick limb bud. *Development* **122**, 1449-1466. doi:10.1242/dev.122.5.1449
Nichols, J. T., Pan, L., Moens, C. B. and Kimmel, C. B. (2013). Barx1 represses joints and promotes cartilage in the craniofacial skeleton. *Development (Cambridge, England)* **140**, 2765-2775. doi:10.1242/dev.090639
Nieto, M. A. (2018). A snail tale and the chicken embryo. *Int. J. Dev. Biol.* **62**, 121-126. doi:10.1387/ijdb.170301mn
Novitch, B. G., Wichterle, H., Jessell, T. M. and Sockanathan, S. (2003). A requirement for retinoic acid-mediated transcriptional activation in ventral neural patterning and motor neuron specification. *Neuron* **40**, 81-95. doi:10.1016/j.neuron.2003.08.006
Olson, L. E., Zhang, J., Taylor, H., Rose, D. W. and Rosenfeld, M. G. (2005). Barx2 functions through distinct corepressor classes to regulate hair follicle remodeling. *Proc. Natl. Acad. Sci. USA* **102**, 3708-3713. doi:10.1073/pnas.0500519102
Oster, G. F., Shubin, N., Murray, J. D. and Alberch, P. (1988). Evolution and morphogenetic rules: the shape of the vertebrate limb in ontogeny and phylogeny. *Evolution* **42**, 862-884. doi:10.2307/2408905
Palmeirim, I., Henrique, D., Ish-Horowicz, D. and Pourquié, O. (1997). Avian hairy gene expression identifies a molecular clock linked to vertebrate segmentation and somitogenesis. *Cell* **91**, 639-648. doi:10.1016/S0092-8674(00)80451-1
Pascoal, S., Carvalho, C. R., Rodriguez-León, J., Delfini, M.-C., Duprez, D., Thorsteinsdóttir, S. and Palmeirim, I. (2007). A molecular clock operates during chick autopod proximal-distal outgrowth. *J. Mol. Biol.* **368**, 303-309. doi:10.1016/j.jmb.2007.01.089
Ray, A., Singh, P. N. P., Sohaskey, M. L., Harland, R. M. and Bandyopadhyay, A. (2015). Precise spatial restriction of BMP signaling is essential for articular cartilage differentiation. *Development* **142**, 1169-1179. doi:10.1242/dev.110940
Reynolds, A., Leake, D., Boese, Q., Scaringe, S., Marshall, W. S. and Khvorova, A. (2004). Rational siRNA design for RNA interference. *Nat. Biotechnol.* **22**, 326-330. doi:10.1038/nbt936
Roh, J.-I., Lee, J., Park, S. U., Kang, Y.-S., Lee, J., Oh, A.-R., Choi, D. J., Cha, J.-Y. and Lee, H.-W. (2018). CRISPR-Cas9-mediated generation of obese and diabetic mouse models. *Exp. Anim.* **67**, 229-237. doi:10.1538/expanim.17-0123
Rolfe, R. A., Nowlan, N. C., Kenny, E. M., Cormican, P., Morris, D. W., Prendergast, P. J., Kelly, D. and Murphy, P. (2014). Identification of mechanosensitive genes during skeletal development: Alteration of genes associated with cytoskeletal rearrangement and cell signalling pathways. *BMC Genomics* **15**, 48. doi:10.1186/1471-2164-15-48
Sachidanandan, C., Yeh, J.-R. J., Peterson, Q. P. and Peterson, R. T. (2008). Identification of a novel retinoid by small molecule screening with Zebrafish embryos. *PLoS ONE* **3**, e1947. doi:10.1371/journal.pone.0001947
Sato, Y., Yasuda, K. and Takahashi, Y. (2002). Morphological boundary forms by a novel inductive event mediated by Lunatic fringe and Notch during somitic segmentation. *Development* **129**, 3633-3644. doi:10.1242/dev.129.15.3633
Sato, K., Koizumi, Y., Takahashi, M., Kuroiwa, A. and Tamura, K. (2007). Specification of cell fate along the proximal-distal axis in the developing chick limb bud. *Development* **134**, 1397-1406. doi:10.1242/dev.02822
Schultz, A. H. (1944). Age changes and variability in gibbons. A Morphological study on a population sample of a man-like ape. *Am. J. Phys. Anthropol.* **2**, 1-129. doi:10.1002/ajpa.1330020102
Scotti, M., Kherdjemil, Y., Roux, M. and Kmita, M. (2015). A *Hoxa13*: Cre mouse strain for conditional gene manipulation in developing limb, hindgut, and urogenital system. *Genesis* **53**, 366-376. doi:10.1002/dvg.22859
Sen, J., Harpavat, S., Peters, M. A. and Cepko, C. L. (2005). Retinoic acid regulates the expression of dorsoventral topographic guidance molecules in the chick retina. *Development* **132**, 5147-5159. doi:10.1242/dev.02100
Shojaei Baghini, S., Gardanova, Z. R., Zekiy, A. O., Shomali, N., Tosan, F. and Jarahian, M. (2021). Optimizing sgRNA to improve CRISPR/Cas9 knockout efficiency: special focus on human and animal cell. *Front. Bioeng. Biotechnol.* **9**, 775309. doi:10.3389/fbioe.2021.775309
Singh, P. N. P., Ray, A., Azad, K. and Bandyopadhyay, A. (2016). A comprehensive mRNA expression analysis of developing chicken articular cartilage. *Gene Expr. Patterns* **20**, 22-31. doi:10.1016/j.gep.2015.11.001
Singh, P. N. P., Yadav, U. S., Azad, K., Goswami, P., Kinare, V. and Bandyopadhyay, A. (2017). NFIA and GATA3 are crucial regulators of embryonic articular cartilage differentiation. *Development* **145**, dev156554. doi:10.1242/dev.156554
Singh, P. N. P., Shea, C. A., Sonker, S. K., Rolfe, R. A., Ray, A., Kumar, S., Gupta, P., Murphy, P. and Bandyopadhyay, A. (2018). Precise spatial restriction of BMP signaling in developing joints is perturbed upon loss of embryo movement. *Development* **145**, dev153460. doi:10.1242/dev.153460
Smith, J. M. and Savage, R. J. G. (1956). Some locomotory adaptations in mammals. *J. Linnean Soc. Lond. Zool.* **42**, 603-622. doi:10.1111/j.1096-3642.1956.tb02220.x
Später, D., Hill, T. P., O'Sullivan, R. J., Gruber, M., Conner, D. A. and Hartmann, C. (2006). Wnt9a signaling is required for joint integrity and regulation of *Ihh* during chondrogenesis. *Development* **133**, 3039-3049. doi:10.1242/dev.02471
Sperber, S. M. and Dawid, I. B. (2008). Barx1 is necessary for ectomesenchyme proliferation and osteochondroprogenitor condensation in the zebrafish pharyngeal arches. *Dev. Biol.* **321**, 101-110. doi:10.1016/j.ydbio.2008.06.004

Storm, E. E. and Kingsley, D. M. (1999). GDF5 coordinates bone and joint formation during digit development. *Dev. Biol.* **209**, 11-27. doi:10.1006/dbio.1999.9241

Tabin, C. and Wolpert, L. (2007). Rethinking the proximodistal axis of the vertebrate limb in the molecular era. *Genes Dev.* **21**, 1433-1442. doi:10.1101/gad.1547407

Tsumaki, N., Nakase, T., Miyaji, T., Kakiuchi, M., Kimura, T., Ochi, T. and Yoshikawa, H. (2002). Bone morphogenetic protein signals are required for cartilage formation and differently regulate joint development during skeletogenesis. *J. Bone Miner. Res.* **17**, 898-906. doi:10.1359/jbmr.2002.17.5.898

Tucker, A. S., Matthews, K. L. and Sharpe, P. T. (1998). Transformation of tooth type induced by inhibition of BMP signaling. *Science* **282**, 1136-1138. doi:10.1126/science.282.5391.1136

Vargesson, N., Kostakopoulou, K., Drossopoulou, G., Papageorgiou, S. and Tickle, C. (2001). Characterisation of hoxa gene expression in the chick limb bud in response to FGF. *Dev. Dyn.* **220**, 87-90. doi:10.1002/1097-0177

Vermot, J., Gallego Llamas, J., Fraulob, V., Niederreither, K., Chambon, P. and Dollé, P. (2005). Retinoic acid controls the bilateral symmetry of somite formation in the mouse embryo. *Science (New York, N.Y.)* **308**, 563-566. doi:10.1126/science.1108363

Wilkinson, D. G. and Nieto, M. A. (1993). Detection of messenger RNA by in situ hybridization to tissue sections and whole mounts. *Methods Enzymol.* **225**, 361-373. doi:10.1016/0076-6879(93)25025-W

Yashiro, K., Zhao, X., Uehara, M., Yamashita, K., Nishijima, M., Nishino, J., Saijoh, Y., Sakai, Y. and Hamada, H. (2004). Regulation of retinoic acid distribution is required for proximodistal patterning and outgrowth of the developing mouse limb. *Dev. Cell* **6**, 411-422. doi:10.1016/S1534-5807(04)00062-0

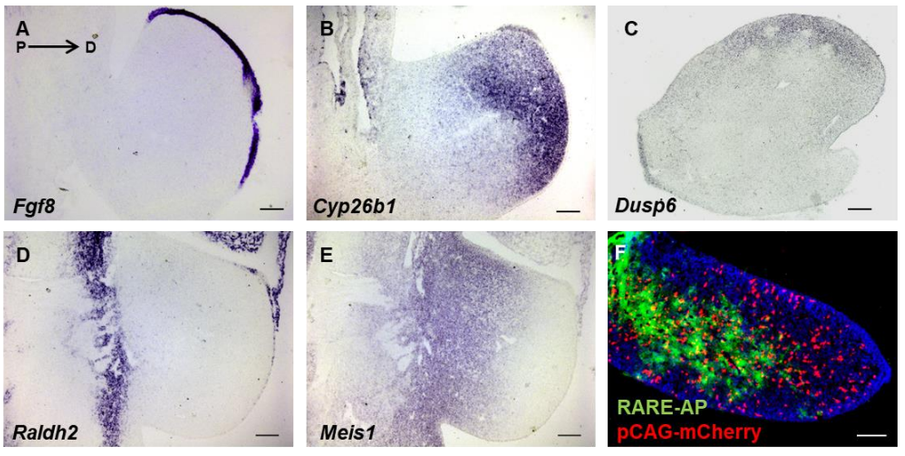

Fig. S1. Reciprocal RA and FGF signaling gradients in a HH23 chick limb bud. (A) *FGF8* expression in Apical Ectoderm Ridge (AER). **(B)** Graded *Cyp26b1* (an FGF signaling downstream target) expression. **(C)** Graded *Dusp6* (an FGF signaling downstream target) expression. **(D)** Expression of RA synthesizing enzyme, *Raldh2* in body flank. **(E)** Graded *Meis1* expression (a RA signaling downstream target). **(F)** Graded RA signaling reporter activity. Scale 100µm.

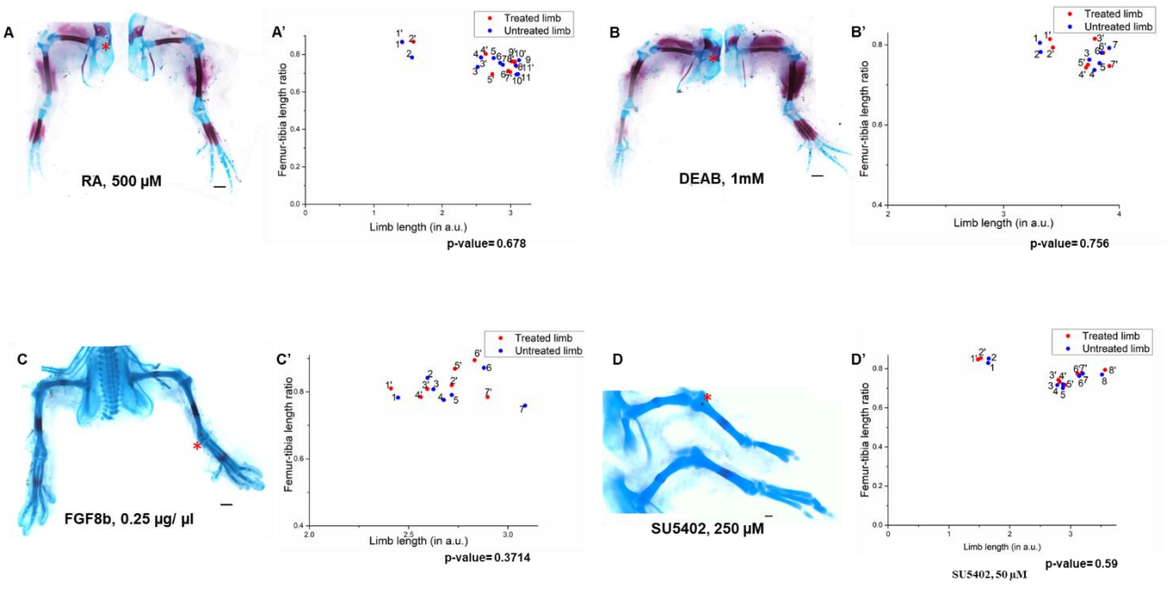

Fig. S2. Perturbation of RA or FGF gradients keeps skeletal elements length ratio unaltered. (A-D) Skeletal preparations from HH21 embryos, with right hind limb-bud implanted with beads RA (10µM) **(A)**, SU5402 (50µM) **(B)**, DEAB (500µM) **(C)**, FGF8 protein (0.1 µg/µl) **(D),** and harvested at around day6-8 of incubation. **(A´- D´)** Graphs representing femur to tibia length ratio (y-axis) and total limb length (x-axis) from treated (hyphenated) and untreated limbs. Treated and Untreated limbs from same embryo labelled by same numeral. Scale 1mm. 1 arbitrary unit (a.u.) equals approx. 5 mm. Red asterisk, bead.

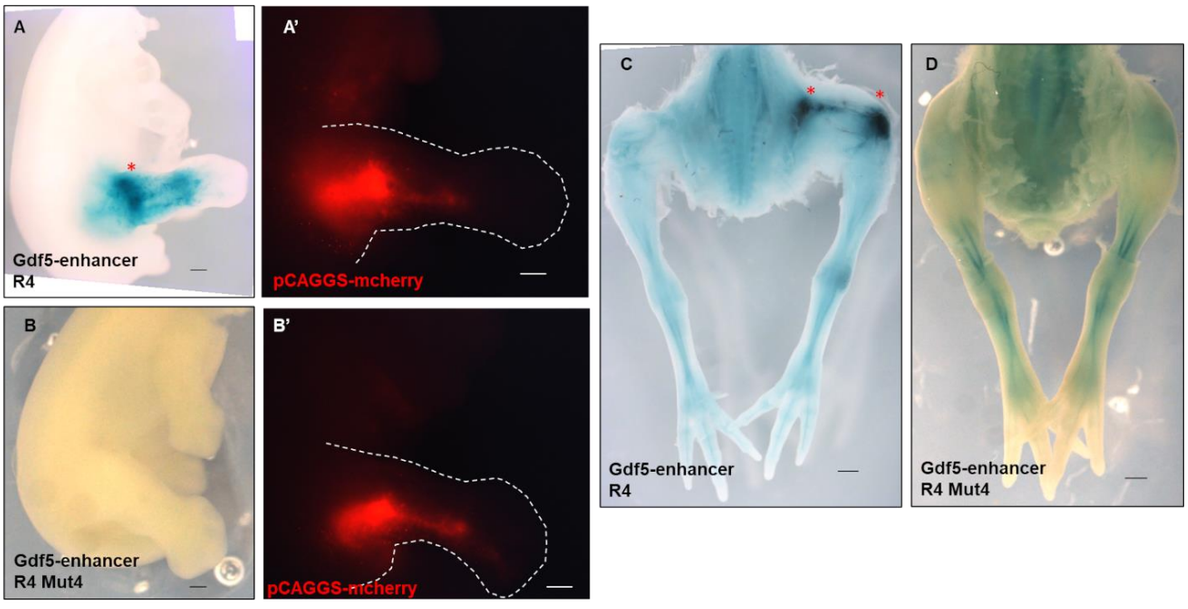

Fig. S3. Loss of Barx binding sites abolishes Gdf5 enhancer (R4) activity. (A-D) LacZ staining in embryos, post *in ovo* electroporation of R4 enhancer **(A** and **C)** and R4 Mut4 enhancer with mutated Barx binding sites **(B** and **D)** at HH28 **(A** and **B)** (n=4) and HH36 **(C** and **D)** (n=3). **(A´,B´)** mCherry signal corresponding to embryos in **(A,B)**. Asterisk, β-galactosidase activity. Scale 1mm.

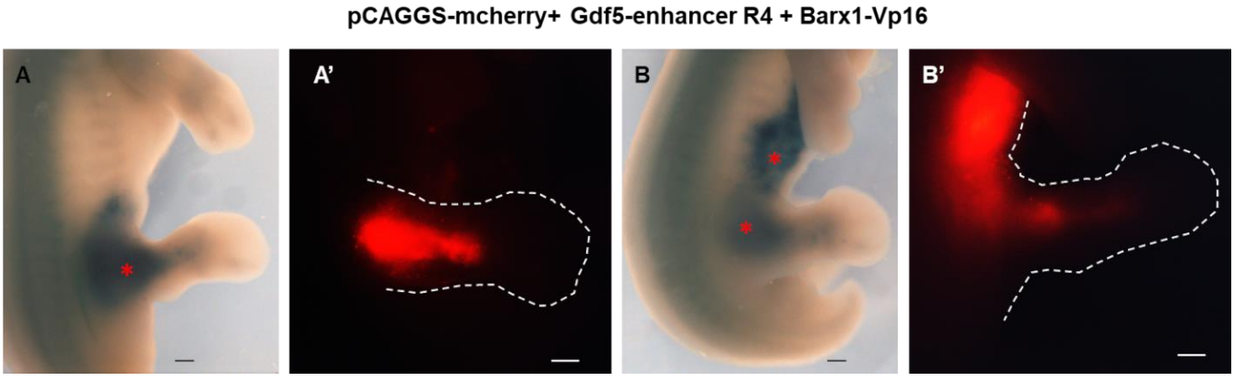

Fig. S4. Constitutively active Barx1 leads to ectopic activation of Gdf5-reporter in HH28 chick limbs. (A, B) LacZ staining in embryos, post *in ovo* electroporation of R4 enhancer and Barx1-Vp16 in limb **(A)** and skin tissue overlying gut **(B)**. **(A´,B´)** mCherry signal corresponding to embryos in **(A,B)**. Asterisk, the sites of ectopic *Gdf5* R4 enhancer activity. n=3.Scale 1mm.

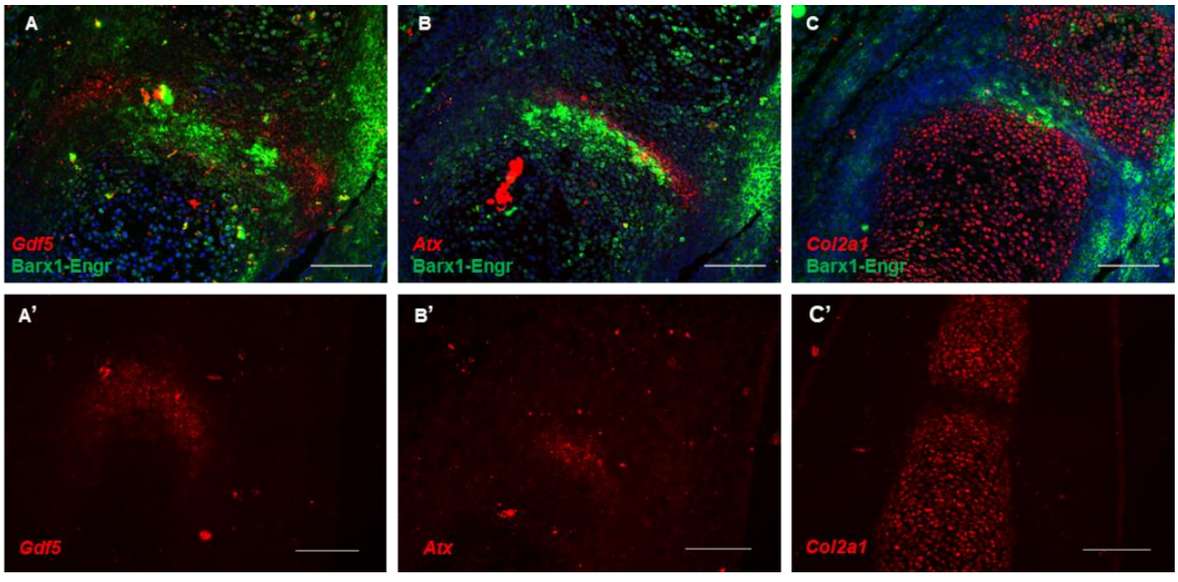

Fig. S5. Loss of Barx1 activity partially abolishes interzone features. Detection of *Gdf5* **(A)**, *Atx* **(B)** and *Col2a1* **(C)** expression. Immunohistochemistry with 3C2 (antibody against the viral gag protein) marks the viral infection domain in green **(A-C)**. *Atx* expression **(A´)**, *Gdf5* expression **(B´)** and *Col2a1* expression **(C´)** in the contralateral control limbs. N=10, Scale 100µm.

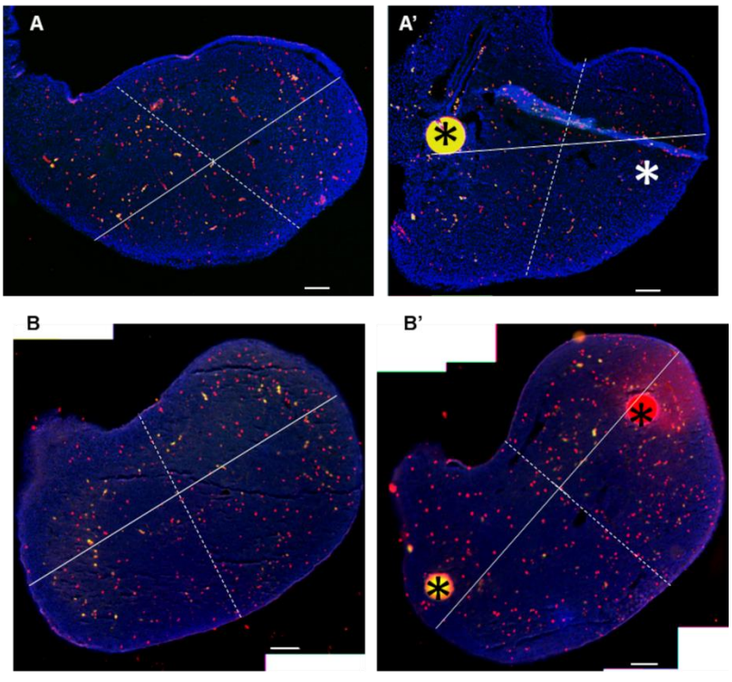

Fig. S6. Cellular proliferation profile upon perturbing RA-FGF signaling gradients. (A,A´) Immunohistochemistry for phosphohistone H3 (pH3) on limb sections treated with RA (10µM) and SU5402 beads (50µM) **(A´)** and contralateral control limbs (**A**). **(B,B´)** Immunohistochemistry for phosphohistone H3 (pH3) on limb sections treated with DEAB (500µM) and FGF8 beads (0.1µg/µl) **(B´)** and contralateral control limbs (**B**). Scale 100µm. Asterisks mark beads.

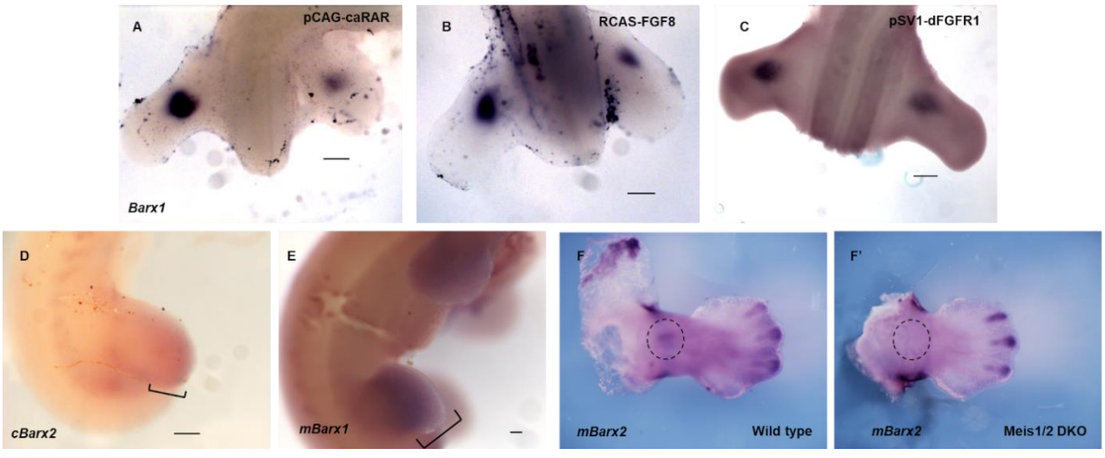

Fig. S7. Up-regulated or down-regulated levels of either RA or FGF signaling suppresses *Barx1* expression. (A-C) Right limb electroporated, pCAG-RAR, n=6 **(A),** RCAS-FGF8, n=6 **(B)**, pSV1-dFGFR1, n=3 **(C)**. **(D**, **E)** *Barx2* and *Barx1* expression in HH24 chick limb bud and E11.5 mice limb bud. **(F**, **F´)** *Barx2* expression in E12.5 wild type, n=3 **(F)** and *Meis1/Meis2* double conditional knockout mice limb buds, n=3 **(F´)**. Scale 300µm.

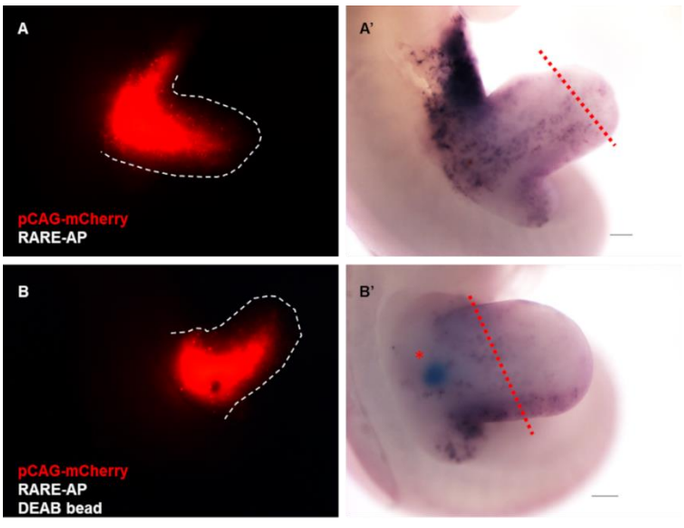

Fig. S8. RA signaling status in developing chick limb bud (HH24), as tested by RARE-AP (A, A´) and its inhibition by DEAB bead application (B, B´). Dashed lines mark extent of RA signaling (n=4). Scale 500µm.

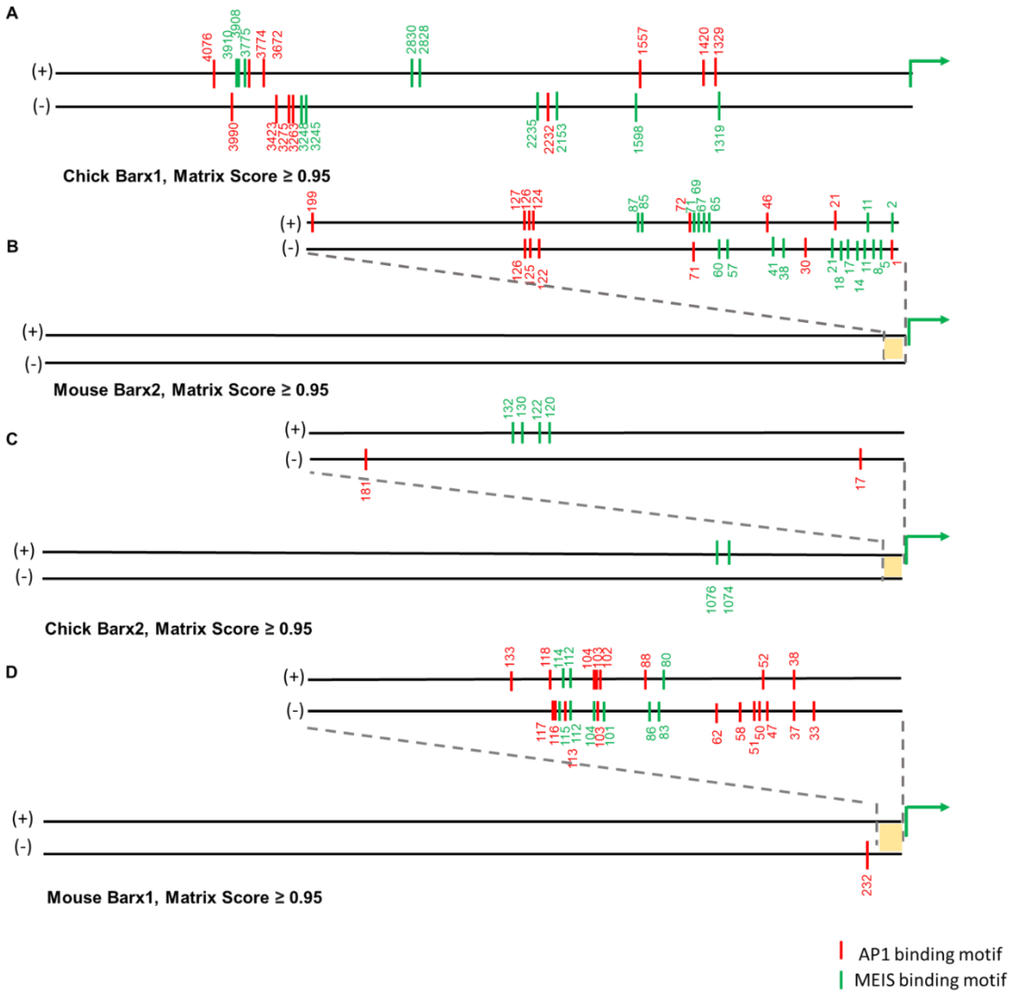

Fig. S9. Putative Barx enhancer analysis. (A-D) 5kb upstream region of chick Barx1 **(A)**, mouse Barx2 **(B)**, chick Barx2 **(C)** and mouse Barx1 **(D)**. AP1 binding sites denoted in red lines and Meis binding sites in green lines in 5kb upstream of chick Barx1 and 200bp upstream of mouse Barx1, chick Barx2, mouse Barx1.

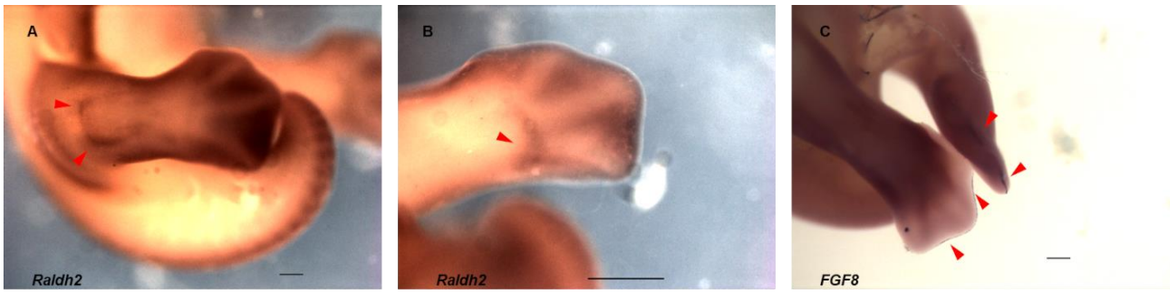

Fig. S10. Raldh2 expresses in newly formed joints in HH30 (A, B) and FGF8 expression persists in limb AER in HH32 (C). Red arrows mark the expression. n=3, Scale 1mm **(A, C)**; n=3, Scale 500µm **(B)**.

Table S1. Changes in femur-tibia length ratios upon implantation of RA and SU5402 beads.

	Treated limb					Untreated limb				
	S	Z	A	S+Z+A	S/Z	S	Z	A	S+Z+A	S/Z
1	0.724	0.723	0.833	2.28	0.998	0.58	0.734	0.826	2.14	0.79
2	0.685	0.652	0.851	2.188	1.05	0.594	0.798	0.832	2.224	0.744
3	0.627	0.664	0.594	1.885	1.06	0.598	0.687	0.809	2.094	0.87
4	0.508	0.519	0.671	1.699	0.983	0.481	0.602	0.678	1.762	0.8
5	0.563	0.551	0.605	1.72	1.02	0.491	0.607	0.671	1.77	0.81
6	0.489	0.504	0.687	1.68	0.97	0.408	0.523	0.779	1.71	0.78
7	1.274	1.637	2.151	5.062	0.778	1.137	1.701	2.128	5	0.668
8	1.177	1.507	1.536	4.22	0.78	1.071	1.531	1.527	4.13	0.7
9	0.476	0.521	0.691	1.688	0.914	0.449	0.529	0.783	1.761	0.849
10	1.152	1.456	1.162	3.77	0.79	0.916	1.55	1.104	3.57	0.59
11	1.38	1.038	1.013	3.433	0.75	0.858	1.432	0.904	3.194	0.59
12	1.022	1.351	0.957	3.33	0.756	0.894	1.414	0.882	3.19	0.632
13	0.403	0.439	0.578	1.42	0.92	0.398	0.508	0.554	1.46	0.78

Table S2. Changes in femur-tibia length ratios upon implantation of DEAB and FGF8 beads.

	Untreated limb					Treated limb				
	S	Z	A	S/Z	S+Z+A	S	Z	A	S/Z	S+Z+A
1	0.779	0.901	0.897	0.865	2.577	0.707	0.921	0.641	0.767	2.269
2	0.762	0.895	0.929	0.851	2.586	0.699	0.893	1.042	0.782	2.634
3	0.791	0.938	1.036	0.843	2.765	0.749	0.95	1.001	0.788	2.7
4	1.568	2.015	2.425	0.778	6.008	1.426	1.957	2.691	0.728	6.074
5	0.543	0.644	0.733	0.843	1.92	0.48	0.63	0.694	0.761	1.804
6	0.945	1.076	1.422	0.86	3.443	0.817	1.123	1.34	0.727	3.28
7	0.49	0.606	0.629	0.81	1.725	0.47	0.63	0.609	0.74	1.704
8	0.836	1.056	1.138	0.792	3.03	0.799	1.08	1.372	0.73	3.251
9	1.012	1.27	1.37	0.797	3.652	0.919	1.255	1.619	0.732	3.793
10	0.715	0.883	0.991	0.81	2.591	0.571	0.817	1.068	0.7	2.457

Table S3. Changes in the lengths proximal and distal to *Barx1* expression upon implantation of RA and SU5402 beads.

	Treated limb				Untreated limb			
	Length proximal to *Barx1* expression (p')	Length distal to *Barx1* expression (d')	Total limb length (p'+d')	Ratio of length proximal and distal to Barx1 expression (p'/d')	Length proximal to Barx1 expression (p)	Length distal to Barx1 expression (d)	Total limb length (p+d)	Ratio of length proximal and distal to Barx1 expression (p/d)
1	0.459	0.454	0.913	1.01	0.411	0.584	0.995	0.703
2	0.476	0.489	0.965	0.973	0.461	0.583	1.044	0.79
3	0.473	0.693	1.166	0.682	0.392	0.785	1.177	0.499
4	0.422	0.463	0.885	0.911	0.409	0.526	0.935	0.778
5	0.302	0.307	0.609	0.98	0.241	0.32	0.561	0.75
6	0.238	0.273	0.511	0.86	0.205	0.291	0.496	0.7
7	0.21	0.235	0.445	0.893	0.202	0.288	0.49	0.7
8	0.233	0.197	0.43	1.1	0.164	0.224	0.398	0.73
9	0.249	0.268	0.517	0.92	0.193	0.275	0.468	0.7
10	0.225	0.235	0.46	0.95	0.172	0.216	0.388	0.79

Table S4. Changes in the lengths proximal and distal to *Barx1* expression upon implantation of DEAB and FGF8 beads.

	Untreated limb				Treated limb			
	Length proximal to *Barx1* expression (p)	Length distal to *Barx1* expression (d)	Total limb length (p+d)	Ratio of length proximal and distal to Barx1 expression (p/d)	Length proximal to Barx1 expression (p')	Length distal to Barx1 expression (d')	Total limb length (p'+d')	Ratio of length proximal and distal to Barx1 expression (p'/d')
1	0.674	0.866	1.54	0.779	0.541	0.948	1.489	0.57
2	0.64	0.72	1.36	0.89	0.468	0.721	1.19	0.65
3	0.513	0.657	1.17	0.78	0.489	0.731	1.22	0.67
4	0.522	0.607	1.13	0.86	0.469	0.661	1.13	0.71
5	0.533	0.667	1.2	0.8	0.43	0.666	1.1	0.65
6	0.657	0.82	1.48	0.8	0.549	0.931	1.48	0.59
7	0.552	0.718	1.27	0.77	0.526	0.863	1.39	0.61
8	0.618	0.782	1.4	0.79	0.482	0.927	1.41	0.52
9	0.711	0.808	1.52	0.88	0.628	0.952	1.58	0.66
10	0.652	0.767	1.42	0.85	0.498	0.831	1.33	0.6
11	0.71	0.899	1.61	0.79	0.626	1.043	1.67	0.6
12	0.279	0.306	0.586	0.912	0.204	0.271	0.475	0.751
13	0.295	0.307	0.602	0.964	0.228	0.332	0.56	0.688

Table S5. Extent of Meis1 expression domain with respect to Barx1 expression domain.

RA-SU5402 beads implantation							
	Length in µm, distal to Barx1 expression (Treated limb)*	Mean	St. Dev	Length in µm, proximal to Barx1 expression (Contralateral Control limb)	Mean	St. Dev	p-value
N=1	303.88			-184.97			
N=2	280.759	269.19	36.781	-171.758	-179.013	11.466	$5.119*10^{-9}$
N=3	208.092			-196.227			
N=4	287.365			-168.334			
N=5	265.895			-173.773			

*Meis1 expression extends distally to Barx1 expression upon RA-SU5402 bead implantation.

DEAB-FGF beads implantation							
	Length in µm, proximal to Barx1 expression (Treated limb)	Mean	St. Dev	Length in µm, proximal to Barx1 expression (Contralateral Control limb)	Mean	St. Dev	p-value
N=1	-228.429			-190.088			
N=2	-291.191	-271.2	37.29	-182.498	-189.26	32.83	0.022
N=3	-311.587			-238.313			
N=4	-253.576			-146.14			

Table S6. Cellular proliferation across limb proximo-distal axis upon perturbation of RA-FGF signaling gradients (number of pH3 positive cells)

	RA-SU5402 bead implantation	
	Untreated limb	Treated limb
N=1 (HH24)	619	587
N=2 (HH24)	658	615
N=3 (HH25)	1097	984
	Untreated Proximal half	Treated Proximal half
N=1	256	238
N=2	277	253
N=3	513	472
	Untreated Distal half	Treated Distal half
N=1	363	349
N=2	381	362
N=3	584	512

	DEAB-FGF8 bead implantation	
	Untreated limb	Treated limb
N=1 (HH25)	998	1165
N=2(HH24-25)	721	873
N=3 (HH25)	1008	1335
	Untreated Proximal half	Treated Proximal half
N=1	467	532
N=2	331	391
N=3	419	615
	Untreated Distal half	Treated Distal half
N=1	531	633
N=2	390	482
N=3	589	720

Table S7. *Barx1* expression Mean Intensity for experiments in Fig. 5 and Fig. S7C:

RA bead at putative Barx1 expression site			
N	Untreated	Treated	p-value
1	60.912	30.8	
2	40.942	25.22	
3	49.22	22.5	
4	42.96	17.185	0.0008
5	37.541	10.173	
6	36.332	10.305	
7	24.204	9.722	

FGF8 bead at putative Barx1 expression site			
N	Untreated	Treated	p-value
1	33.83	10.992	
2	51.79	12.929	
3	54.975	20.839	0.0002
4	41.32	16.647	
5	78.875	20.285	
6	72.649	27.669	
7	56.589	33.468	

dnRAR *in ovo* electroporation			
N	Untreated	Treated	p-value
1	150.681	132.574	
2	124.791	111.582	0.0329
3	157.468	118.744	
4	137.858	110.585	

dnMKK1 *in ovo* electroporation			
N	Untreated	Treated	p-value
1	67.318	24.799	
2	66.026	37.26	0.0019
3	59.998	34.767	

DEAB bead only in limb proximal			
N	Untreated	Treated	p-value
1	74.694	51.369	
2	85.225	61.175	0.03953
3	53.463	51.309	
4	97.225	62.849	
5	101.266	70.396	

SU5402 bead only in limb distal			
N	Untreated	Treated	p-value
1	110.731	89.263	
2	84.232	64.74	
3	80.342	72.522	0.025
4	113.255	58.569	
5	122.727	85.528	

DEAB-SU5402 bead implantation at HH22-23						
N	Untreated limb, Endogenous Barx1 expression intensity	Treated limb, Endogenous Barx1 expression intensity	p-value	Untreated limb, intensity at comparable region	Treated limb, Ectopic Barx1 expression intensity	p-value
1	121.23	101.226		13.207	90.046	
2	134.299	133.952		26.139	140.048	
3	157.364	136.52		97.426	125.2	
4	103.78	67.37		28.117	73.839	
5	140.714	97.095		45.789	119.63	
6	95.215	78.131	0.046	23.61	110.198	0.000023
7	163.338	81.044		31.187	58.123	
8	138.39	123.496		87.237	102.179	
9	141.754	130.194		43.222	112.235	
10	106.371	98.128		10.42	88.67	
11	99.608	97.941		15.206	62.996	
12	98.237	92.702		48.575	78.518	
13	73.382	39.708		47.087	63.592	

DEAB-SU5402 bead implantation at HH20-21						
N	Untreated limb, Endogenous Barx1 expression intensity	Treated limb, Endogenous Barx1 expression intensity	p-value	Untreated limb, intensity at comparable region	Treated limb, Ectopic Barx1 expression intensity	p-value
1	18.388	17.653		10.298	35.631	
2	37.894	16.754		16.606	48.681	
3	38.864	18.887	0.00968	7.029	36.771	0.000289
4	36.109	17.138		13.415	66.835	
5	40.63	26.416		3.724	56.077	

***in ovo* electroporation of pSV1-dFGFR1**							
	Untreated	Mean	St. Dev	Treated	Mean	St. Dev	p-value
N=1	68.482			50.935			
N=2	56.78	63.054	5.896	46.87	48.6	2.097	0.0161
N=3	63.9			48.007			

Click here to download Table S7